

Single-Atom Catalysis

How to cite: *Angew. Chem. Int. Ed.* **2021**, *60*, 13177–13196

International Edition: doi.org/10.1002/anie.202014112

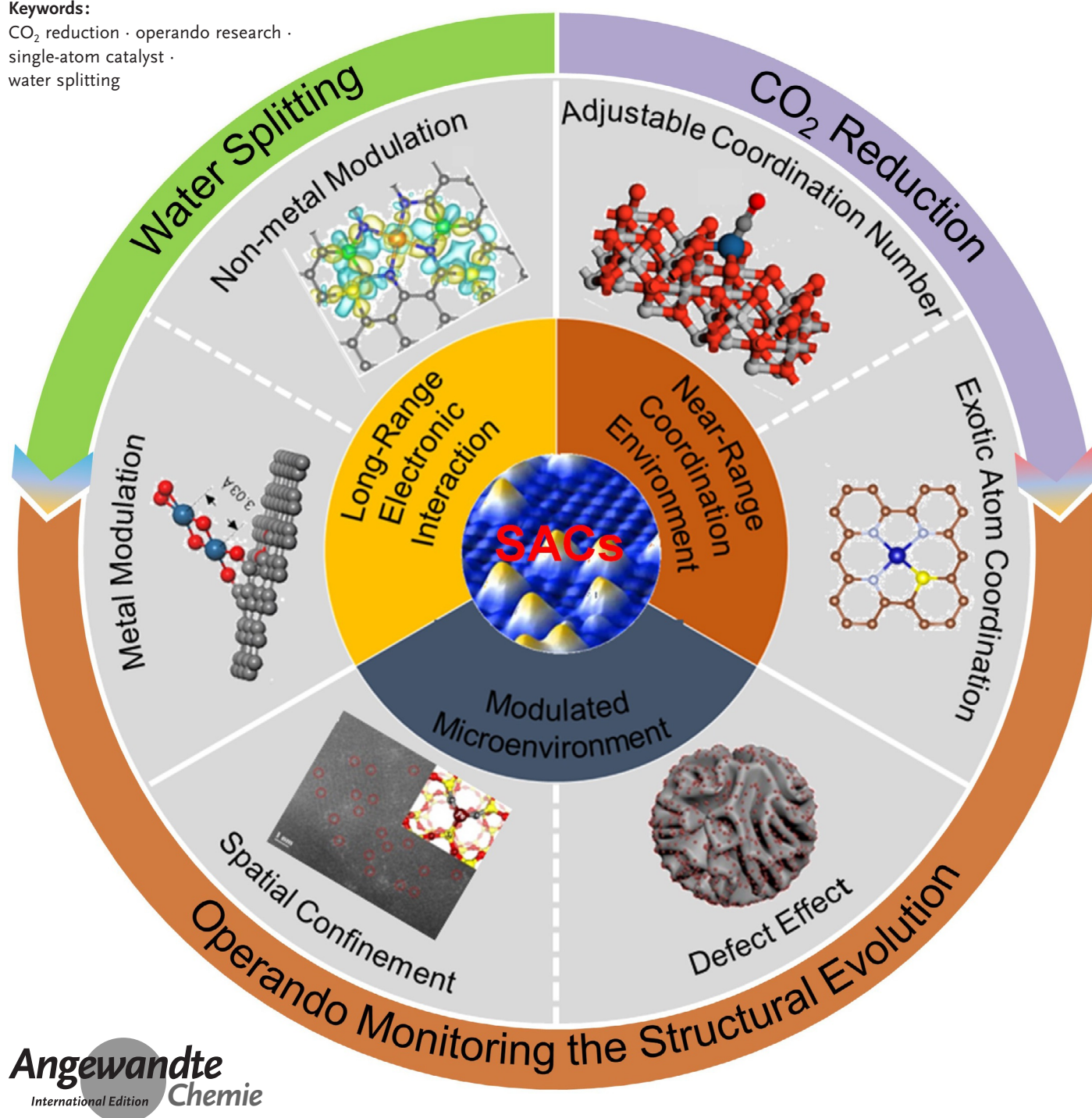
German Edition: doi.org/10.1002/ange.202014112

Atomically Dispersed Reactive Centers for Electrocatalytic CO₂ Reduction and Water Splitting

Huabin Zhang, Weiren Cheng, Deyan Luan,* and Xiong Wen (David) Lou*

Keywords:

CO₂ reduction · operando research · single-atom catalyst · water splitting



Developing electrocatalytic energy conversion technologies for replacing the traditional energy source is highly expected to resolve the fossil fuel exhaustion and related environmental problems. Exploring stable and high-efficiency electrocatalysts is of vital importance for the promotion of these technologies. Single-atom catalysts (SACs), with atomically distributed active sites on supports, perform as emerging materials in catalysis and present promising prospects for a wide range of applications. The rationally designed near-range coordination environment, long-range electronic interaction and microenvironment of the coordination sphere cast huge influence on the reaction mechanism and related catalytic performance of SACs. In the current Review, some recent developments of atomically dispersed reactive centers for electrocatalytic CO₂ reduction and water splitting are well summarized. The catalytic mechanism and the underlying structure–activity relationship are elaborated based on the recent progresses of various operando investigations. Finally, by highlighting the challenges and prospects for the development of single-atom catalysis, we hope to shed some light on the future research of SACs for the electrocatalytic energy conversion.

1. Introduction

The development of renewable and efficient energy conversion technologies is a necessary requirement to meet the growing demand of energy consumption and environmental protection.^[1–5] Among various types of energy conversion approaches, electrochemical CO₂ reduction and water splitting have been proven as promising strategies for their environmental benignancy and high efficiencies.^[6–10] As demonstrated, the efficiency of the above-mentioned energy conversion approaches is highly related to the sluggish kinetics of the rate-determining step.^[11–14] In this regard, developing durable and highly efficient electrocatalysts is of vital importance to accelerate the reaction kinetics and thus improve the overall energy conversion efficiency. At present, precious metal-based catalysts (e.g., Au, Pt, RuO₂ and IrO₂) are verified as the most efficient electrocatalysts for many energy conversion processes, but the scarcity and high cost severely hinder their large-scale applications.^[15–17] Therefore, developing cost-efficient and highly active electrocatalysts is one ideal direction for promoting clean energy conversion technologies.^[18–21]

The catalytic efficiency of the electrocatalyst relies greatly on two elements. They are the number of reactive centers and the intrinsic activity of individual reactive sites.^[22–25] With the diminishing of the catalyst size, more reactive sites are exposed and thus greatly boosting the total number of the reactive centers.^[26,27] On the other hand, greatly enhanced intrinsic activity for the individual site can be realized by tuning the electronic structure and coordination sphere.^[28–30] Atomically dispersed reactive centers in particular configurations represent the maximized atom utilization for metal species and meanwhile improve the intrinsic catalytic activity

of the individual sites.^[31–33] Single-atom catalysts (SACs) with tunable electronic structure and unsaturated coordination deliver superior catalytic performance in varied catalytic processes.^[34–37] Moreover, the homogeneity of the isolated active sites in SACs provides an ideal model for monitoring the structural evolution of the reactive centers under realistic conditions.^[38,39] In-depth comprehension of the complicated reaction kinetics can thus be proposed, which is very helpful in gaining hints about the nature of reactive centers.^[40,41] Real-time monitoring of isolated reactive centers via operando experiments is also highly beneficial for revealing the interaction between the reactive centers and reactants, thus facilitating the construction of catalysts with optimized activity.

In this Review, some recent breakthroughs in modulating coordination spheres of SACs for improving the catalytic performances are thoroughly summarized. We emphasize the deep insight into the structure–performance relationship via precisely modulating the coordination environment of the isolated reactive centers. Furthermore, the great progresses of applying SACs for CO₂ reduction reaction (CO₂RR) and water splitting are highlighted. In particular, operando characterizations that provide the potential to dynamically monitor the structural evolution of the reactive centers in SACs are elaborated (Figure 1). Finally, some challenges and research perspectives for the cognition of catalytic mechanisms and the rational design of SACs are presented. We aim to offer illustrative accounts on recent progress and rationalize our understanding on this research field, and thus provide fundamental principles and horizons for the further development of single-atom catalysis.

[*] Dr. H. Zhang, Dr. W. R. Cheng, Dr. D. Y. Luan, Prof. X. W. Lou
School of Chemical and Biomedical Engineering, Nanyang Technological University
62 Nanyang Drive, Singapore 637459 (Singapore)
E-mail: dyluan@ntu.edu.sg
xwlou@ntu.edu.sg
Homepage: <https://personal.ntu.edu.sg/xwlou/>

 The ORCID identification number(s) for the author(s) of this article can be found under:
<https://doi.org/10.1002/anie.202014112>.

 © 2020 The Authors. Angewandte Chemie International Edition published by Wiley-VCH GmbH. This is an open access article under the terms of the Creative Commons Attribution Non-Commercial License, which permits use, distribution and reproduction in any medium, provided the original work is properly cited and is not used for commercial purposes.

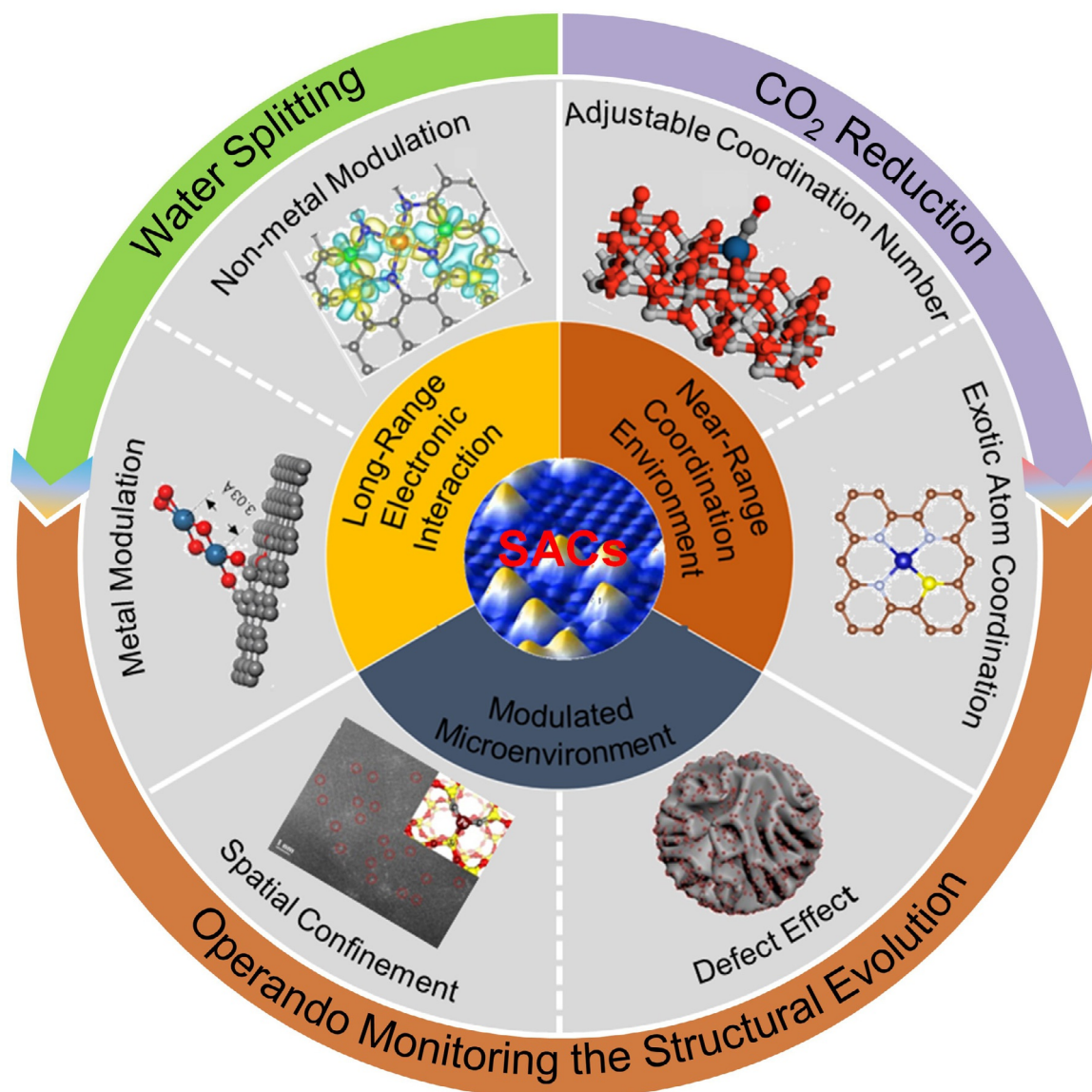


Figure 1. Schematic description of atomically dispersed reactive centers for electrocatalytic CO₂ reduction and water splitting.

2. Modulations for the coordination sphere and microenvironment of SACs

In SACs, the reactive centers are atomically dispersed over the support. They represent the maximized atomic

utilization efficiency and always deliver impressive catalytic performances for various reactions.^[42,43] As a matter of fact, the isolated reactive centers in SACs are not totally isolated. They are always coordinated and stabilized by the adjacent atoms from the support to minimize the high surface energy.



Huabin Zhang received his Ph.D. degree in physical chemistry from University of Chinese Academy of Science in 2013. He is currently a research fellow in Prof. Xiong Wen (David) Lou's group in the School of Chemical and Biomedical Engineering at Nanyang Technological University, Singapore. His research interests focus on advanced catalysis for sustainable energy.



Xiong Wen (David) Lou received his B.Eng. (1st class honours) (2002) and M.Eng. (2004) degrees from the National University of Singapore. He obtained his Ph.D. degree in chemical engineering from Cornell University in 2008. He is currently the Cheng Tsang Man Chair Professor in Energy at Nanyang Technological University, Singapore. His current research is focused on the design and synthesis of nanostructured materials for different applications in batteries, electrocatalysis and photocatalysis.

Thus, the local coordination sphere of SACs could cast significant influence on both selectivity and activity of the particular reaction process.^[44] In general, there are two approaches to modulate the coordination sphere of the reactive centers. One is the direct tuning of the near-range coordination environment of the individual reactive centers. The other is to explore the long-range interactions between heteroatoms on the substrate for modulating the electronic structure. Besides, the microenvironment for the coordination sphere is also a crucial element for influencing the catalytic performance.

2.1. Near-range coordination environment of the isolated reactive centers

As the isolated reactive centers are stabilized by ionic or covalent interaction with the support, the electronic and geometric properties of isolated atoms should be predominantly determined by the local coordination chemistry. Coordination number and coordinated species are two important parameters to determine the near-range coordination sphere of the isolated reactive centers.

2.1.1. Adjustable coordination number of isolated sites

The coordination number of the reactive center has been regarded as an effective descriptor to reflect the structure-performance relationship for SACs, and is also a critical factor for dictating the catalytic activity.^[45] Many approaches have been explored to regulate the coordination number of reactive centers. As an example, varying the calcination temperature of cobalt-based zeolitic imidazolate frameworks can be applied for controlling the number of Co-N coordination in the graphitic carbon matrix-supported SACs.^[46] (Figure 2a–c). The CO₂ reduction investigations confirm that the atomically distributed Co catalysts deliver enhanced activity and selectivity with the decrease in the number of coordinated N atoms from 4 to 2. Density-functional theory (DFT) calculations verify that the Co atom with lower N coordinated number possesses more unoccupied 3d orbitals, giving rise to the facile formation and strong adsorption of CO₂, and thus improving the overall CO₂ reduction efficiency.

For oxide-supported SACs, the isolated active centers are coordinated by oxygen atoms from the support. Comparing with M-C/N coordination, the M-O interaction is even more rigid due to the highly crystalline structure of the oxide support. Zhang and co-worker have developed an efficient synthesis strategy for decorating the isolated Pt atoms onto the support of Fe₂O₃.^[47] The Pt atoms are chelated by the ethylenediamine ligands and then released by removing the ethylenediamine through a rapid thermal treatment in an inert atmosphere (Figure 2d). The coordination number of the isolated Pt centers can be well tuned by changing the thermal treatment temperature. The decrease in Pt-O coordination number results in the decline of the oxidation state of Pt. The hydrogenation activity is thus boosted to a record-high level without sacrificing the product selectivity. The authors conclude that the coordination number of Pt-O in the

first shell determines the oxidation state of the isolated Pt atom, and also influences the catalytic performance of the reactive center.

2.1.2. Exotic atoms in the near-range coordination sphere.

Introducing the exotic atoms into the coordination sphere is a practical way to adjust the electronic structure of the reactive center, which may greatly modulate the catalytic performance. Zhang and co-workers have introduced N atom into the coordination sphere of isolated Ni atoms on the graphene (denoted as HCM@Ni-N).^[48] Extended X-ray absorption fine structure (EXAFS) and X-ray absorption near-edge structure (XANES) spectra investigations confirm that the isolated Ni atoms in HCM@Ni-N are stabilized by Ni-N coordination in unsaturated coordination geometry. DFT calculation verifies that the electronic structure of the hybrid is greatly modified after introducing N atoms into the coordination sphere. The effective electronic coupling between Ni and coordinated N atoms can modify the Fermi level and lower the adsorption energy of intermediates, resulting in the highly accelerated oxygen evolution reaction (OER) kinetics. Han et al., have further introduced the Cl atoms into the near-range coordination sphere, producing an atomically dispersed FeCl₁N₄ site catalyst.^[49] Great improvement in the oxygen reduction in alkaline media has been achieved. The authors attribute the pronounced enhancement in performance to the introduction of the Cl atoms into the coordination sphere, which greatly modulates the electronic state of the isolated Fe reactive center. The coordination geometry of the isolated reactive centers can also be further modulated via the axial coordination assembly. Tang and co-workers have assembled the axial pyridine into the tetra(4-pyridyl) porphyrin cobalt center and confirmed that the axial coordination can increase the Lewis basicity of the reactive Co center.^[50] Moreover, the d_{z²} energy level in Co 3d orbital is significantly elevated after the axial coordination, resulting in greatly improved activity for CO₂ reduction with the Faradaic efficiency of 96 % at the overpotential of 500 mV.

In addition to the well-developed M-N_x centers, single-atom metal-phosphorus-carbon (M-P-C) catalyst with P atoms as the anchor sites has also been established recently. Li and co-workers have successfully decorated the FeP₄ units into the graphitic carbon matrix (Figure 2e).^[51] The developed hybrid delivers excellent catalytic performance and reaction generality in the heterogeneous reductive amination reactions. In contrast, the catalytic performance of the FeN₄ decorated carbon matrix is rather poor and nearly undetectable. This work offers the understanding of heterogeneous M-P-C SACs, and broadens the application of non-metal modulated electronic interactions for adjusting the catalytic performance.

The introduction of exotic atoms does not always generate positive effect on the catalytic kinetics. Wang and co-workers have developed a template-assisted strategy to decorate varied metal atoms into the porous N, S-codoped carbon (NSC) matrix (Figure 2f).^[52] Further structural investigations confirm the existence of direct Ni-S/Co-S bonding in the Ni/Co-centered SACs (Ni-SAC/NSC and Co-SAC/NSC), while

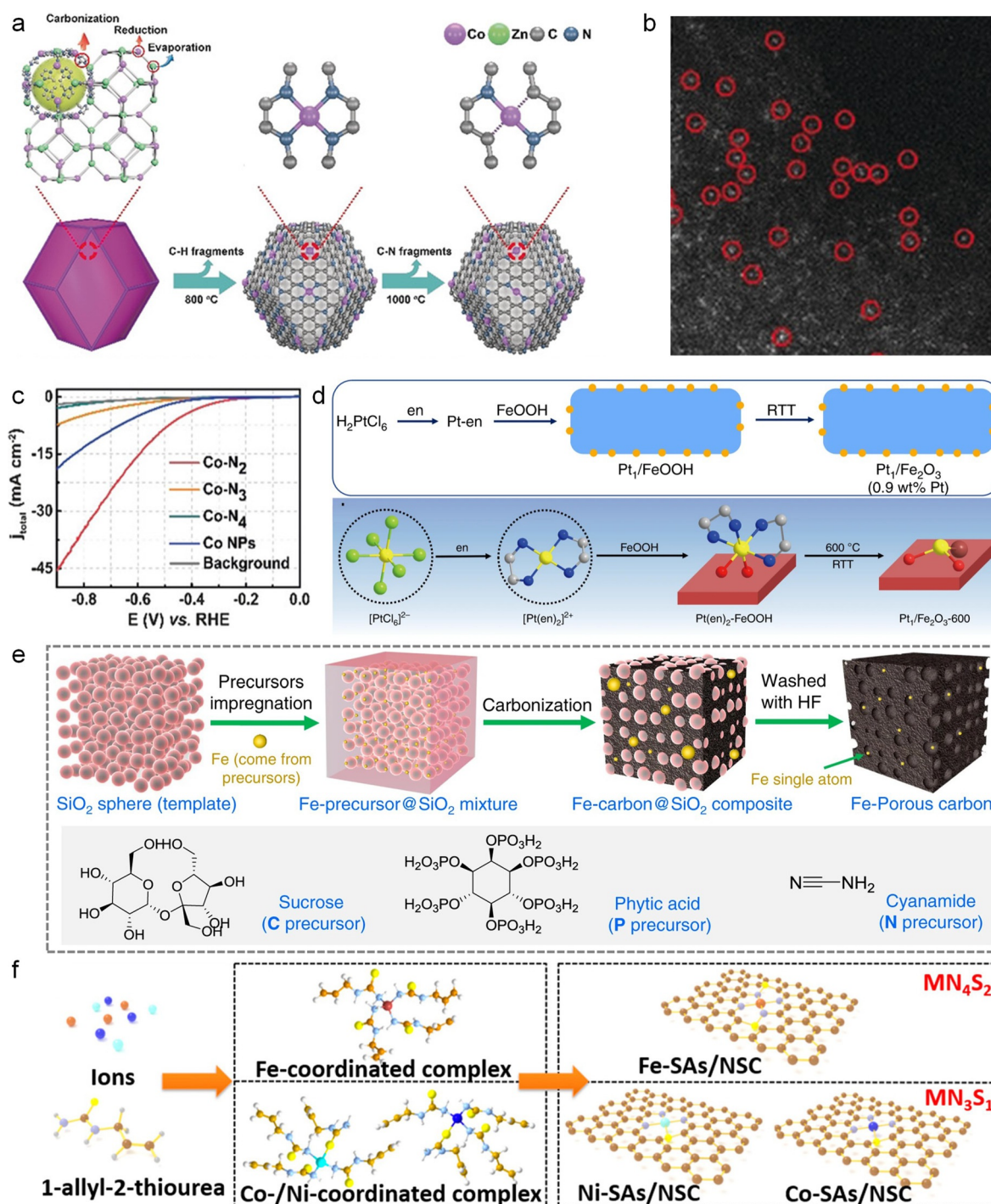


Figure 2. (a) The formation process of hybrids with different coordination numbers. (b) Isolated Co atoms are observed in the magnified high-angle annular dark field scanning transmission electron microscopy (HAADF-STEM) images of Co-N₂. (c) Polarization curves for the CO₂ reduction of varied catalysts.^[46] Copyright 2018, Wiley-VCH Verlag GmbH & Co. KGaA, Weinheim. (d) Schematic description for the structural evolution of Pt species in the synthesis process.^[47] Copyright 2019 Nature Publishing Group. (e) Schematic description for the synthesis of phosphorus species coordinated Fe SAC.^[51] Copyright 2020 Nature Publishing Group. (f) Schematic illustration of the construction of SACs with S participated coordination sphere.^[52] Copyright 2019 Nature Publishing Group.

only Fe-N coordination is observed in the Fe-centered Fe-SAC/NSC. Comparing with the Ni-SAC/NSC and Co-SAC/NSC, the Fe-SAC/NSC without the Fe-S bonding delivers the best catalytic performance in the electrocatalytic oxygen reduction process. The authors conclude that the M-S

bonding in the first coordination sphere should be responsible for the higher energy barriers of the intermediates, resulting in decreased oxygen reduction efficiency.

2.2. Long-range electronic interaction for the isolated reactive centers

The underneath substrates in SACs have been demonstrated as unique templates for modulating the isolated reactive centers by molecular self-assembly, and thus provide elegant platforms to tailor the long-range electronic interactions for the isolated reactive centers. Besides, the communicative effects between active sites have also been claimed as common and indispensable mechanisms in tuning the local electronic fields.

2.2.1. Non-metal modulated electronic interaction

Doping non-metal atoms into the skeleton of the support can efficiently improve electronic features of SACs. Li et al. have emphasized the key role of S heteroatoms in modulating the electronic interaction and the electronic structure of individual metal centers (Figure 3 a).^[53] Comparing with the single-atom Fe catalyst (FeN₄/CN) without S doping in the support, the isolated Fe atoms in the S-doped carbon matrix exhibit greatly enhanced oxygen reduction activity in acidic electrolyte. Experimental results and DFT calculation suggest that the tunable adjacent chemical environments endow the active Fe centers with varied electronic states and optimized binding strength with O₂, resulting in the exceptional improvements for oxygen reduction. By controlling the electron withdrawing/donating properties of carbon plane, Lee and co-workers have further demonstrated that the incorporation of sulfur functionalities into the carbon plane can effectively tune and enhance the kinetic activity of a single Fe-N₄ site.^[54] More specifically, the newly decorated functionalities change the strength of the electronic effect, which is derived from the delocalized π -band of carbon plane to the d-orbital of the Fe ion in Fe-N₄ site, resulting in the change of ORR activity of the Fe-N₄ site. They also conclude that the decoration of charge-donating sulfur functionalities (thiophene-like S) results in lower ORR activity while the introduction of charge-withdrawing groups (oxidized S) may render the catalyst with higher activity.

Jiang and co-workers have developed an atomic interface approach to synthesize Cu-based SAC.^[55] As demonstrated by the X-ray absorption fine structure (XAFS) analyses, the Cu atoms are stabilized by surrounding N atoms from the N, S codoped carbon matrix (Cu-SA/SNC). Experimental results and DFT calculation demonstrate that the indirect interaction between Cu and S atoms within the carbon support significantly decreases the reaction free energy of the adsorbed intermediates and thus boosts the oxygen reduction activity.

2.2.2. Metal modulated electronic interaction

Developing the communication between two neighboring metal monomers is a practical strategy to optimize the catalytic performance and deepen our comprehensive understanding on heterogeneous catalysis. Zeng and co-workers have verified that the synergetic interaction between neighboring Pt monomers induces distinct reaction paths and delivers greatly improved catalytic performance in the CO₂

hydrogenation.^[56] CO₂ can be successively converted into methanol with the metal modulated electronic interaction from neighboring Pt monomers. In contrast, only the conversion of CO₂ into formic acid is realized over the isolated Pt centers. It is concluded that metal modulated electronic interaction varies the reaction barriers, resulting in greatly accelerated reaction kinetics. Moreover, neighboring Pt monomers experience different reaction paths from those isolated monomers. The research finding of the synergetic interaction between neighboring monomers is anticipated to build an advanced approach for manipulating the catalytic performance and deepen the understanding of the heterogeneous catalytic mechanism.

Lu and co-workers have applied the atomic layer deposition method for fabricating Pt₂ dimers on graphene.^[57] The secondary Pt atom can be selectively attached to the primary one through proper nucleation site creation. XAFS and theoretical calculations confirm that the Pt₂ dimers are bridged by the O atoms, instead of coordinated directly through the Pt–Pt bonding. Pt₂ dimers deliver an impressive conversion rate (2800 mol-H₂/mol-Pt⁻¹ min⁻¹) in hydrolytic dehydrogenation of ammonia borane. This value is about 45 and 17-fold higher than those of graphene supported Pt nanoparticles and SACs, respectively. The authors believe that the work offers more possibilities in exploring the metal modulated electronic interactions for adjusting the catalytic performance.

2.3. Tunable microenvironment of the coordination sphere

The steric and chemical microenvironments of isolated reactive centers heavily influence the catalytic activity through extended coordination sphere interactions.^[58,59] Moreover, the enhancement in the selectivity of SACs towards certain targeted products can be realized by altering the reaction pathway, which is also greatly influenced by the steric and chemical microenvironments.

2.3.1. Spatial confinement for the reactive centers

Active centers confined in nanopores often exhibit unusual catalytic behaviors, which are markedly different from those active sites over the surface of supports. Matrixes with uniform pore shapes and sizes are ideal supports for confining reactive centers. Porous zeolites, metal-organic frameworks (MOFs) and porous carbon matrixes have been selected for encapsulating the isolated reactive centers.^[60-62] Li and co-workers have isolated metal sites in Y zeolite by confining a metal-ethylenediamine complex into β -cages during the crystallization process.^[60] Han and co-workers have provided the first direct evidence for the atomic distribution of isolated Mo atoms in the channels of zeolite ZSM-5 via the integrated differential phase-contrast scanning transmission electron microscopy (Figure 3 b).^[63] They also demonstrate the crucial role of the framework in driving the atomic distribution of Mo species in the micropores via the special Mo-Al interaction. Ye and co-workers have isolated Co atoms in the porphyrin units of the well-known MOF-525

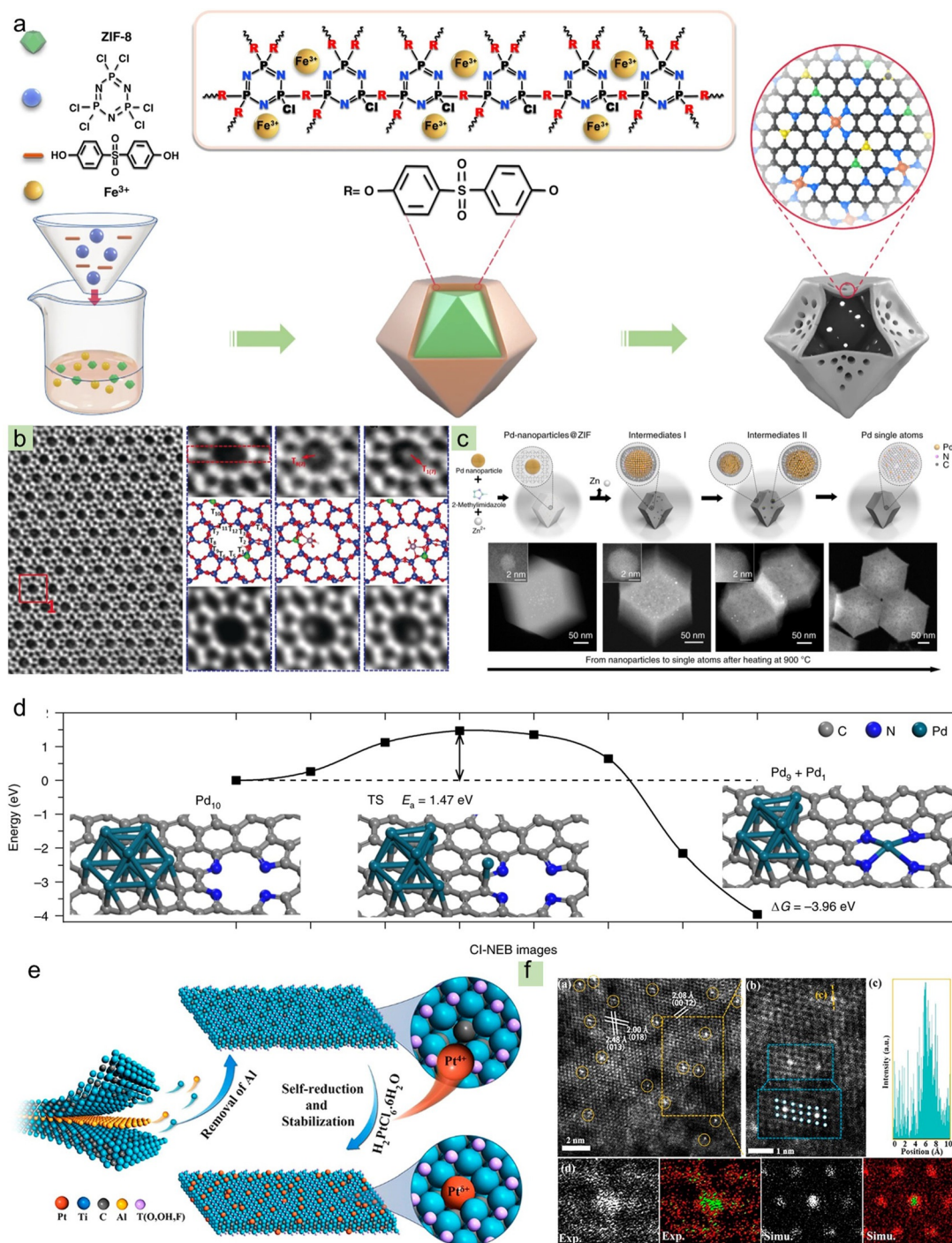


Figure 3. (a) Schematic illustration of the construction of SACs with N, P and S co-doped support.^[53] Copyright 2020 Nature Publishing Group. (b) Presentation for the existence of isolated Mo centers in zeolite channels.^[63] Copyright 2020, Wiley-VCH Verlag GmbH & Co. KGaA, Weinheim. (c) Schematic description for the transformation of isolated Pd atoms from the Pd particle.^[73] Copyright 2018 Nature Publishing Group. (d) Calculated energy diagram for the stretching pathway from Pd particles to isolated Pd atoms.^[73] Copyright 2018 Nature Publishing Group. (e) Self-reduction stabilization process for the preparation of Pt₁/Ti_{3-x}C₂T_y (f) HAADF-STEM characterization for the isolated Pt atoms decorated MXene.^[74] Copyright 2019 American Chemical Society.

and applied the developed hybrid for photocatalytic CO₂ reduction.^[64] The isolated reactive centers adopt unsaturated configurations and are confined in the MOF matrix, which greatly enhance the CO₂ adsorption capacity and reduction efficiency.

As the reaction path may be changed due to the space confining, spatial confinement plays an important role in the selectivity for the generated products. Bao and co-workers confine the isolated Fe atoms into a silica matrix and thus realize the nonoxidative and direct conversion of methane

exclusively to ethylene and aromatics.^[65] In the methane conversion process, cleaving the first C–H bond while suppressing further catalytic dehydrogenation is an effective strategy for avoiding both CO₂ generation and coke deposition, but of course very challenging. The confined Fe sites can activate CH₄ and generate methyl radicals in the absence of oxidants. These generated methyl radicals desorb from the catalyst surface and then experience complicated gas-phase reactions to yield ethylene, benzene and naphthalene. The authors conclude that the spatial confinement of the reactive center is a sustainable approach in the direct CH₄ conversion.

2.3.2. Defective supports for isolated reactive centers

Defects are common in catalysts and can greatly influence the electronic structure and related catalytic performance.^[66–68] Recent investigations have confirmed the existence of defects may cast some positive effects on the catalytic performances. Wang and co-workers have summarized some of research advances of defects and elaborated the role of defects in the electrocatalytic energy conversion processes.^[69] With the introduction of defects, the electronic structures of the hybrids are greatly modified, resulting in boosted electron/charge transfer capacity and reaction kinetics.^[70] Zhang and co-workers have successfully decorated isolated Ru atoms into the carbon matrix with abundant defects.^[71] The as-synthesized hybrid exhibits high catalytic activity and low overpotential for electrocatalytic hydrogen evolution. The authors conclude that defects lead to the enhanced local electric field around the Ru centers thus resulting in the further improved intrinsic activity of SACs.

In addition to the greatly activated electrochemical processes via the defect engineering, defects can also provide unique anchor sites for stabilizing the metal species.^[72] Li and co-workers have confirmed that the defects on graphene can capture the emitted Pd atoms during the calcination process (Figure 3c,d).^[73] The conversion from nanoparticles to the isolated reactive centers is thus realized by capturing the emitted Pd species on the defects of carbon matrix. As confirmed by EXAFS analysis, thermodynamically stable Pd-N₄ configuration is constructed. Chen and co-workers have stabilized the isolated Pt atoms into the two-dimensional Ti_{3-x}C₂T_yMXene nanosheets with abundant Ti defects (Figure 3e,f).^[74] Strong metal-carbon bonds are formed between the Ti defect confined Pt atoms and the Ti_{3-x}C₂T_y support.

3. SACs for electrocatalytic water splitting

Electrocatalytic water splitting has been regarded as one of the most promising approaches for producing hydrogen under mild conditions without the greenhouse gas emission.^[75] Moreover, electrocatalytic water splitting helps mitigate the problematic intermittency of some renewable energies (e.g., solar, wind) by storing the electricity in the form of chemical energy. Water splitting is comprised of two half-cell reactions: OER and hydrogen evolution reaction (HER).^[76] Traditionally, water splitting is realized in the typical electrolysis cell, in which these two half-reactions

occur simultaneously on two electrodes: H₂ is generated in the cathode while the water is oxidized to O₂ at the anode.^[21,77,78] Despite many progresses achieved on electrocatalytic water splitting, highly active and durable catalysts have to be developed to overcome the kinetic barriers in the water splitting process, especially for the OER.^[79]

3.1. HER

Hydrogen generation via electrocatalytic water splitting is an ideal approach for exploring clean energy. Pt delivers the best activity among various electrocatalysts for hydrogen evolution, but its widespread application is greatly hindered by the high cost and scarcity.^[80–82] Developing alternative electrocatalysts with superior activity and low cost represents an elegant solution to enable the hydrogen economy. SACs featuring atomically dispersed reactive centers on the conductive support have emerged as promising electrocatalysts for HER.^[83]

Lou and co-workers have relocated the isolated Pt species from the surface of the support into the interior of the carbon matrix by high temperature calcination under inert atmosphere (Figure 4a–d).^[61] Mesoporous polydopamine particles and surface adsorbed Pt species are applied as the precursor for constructing the isolated Pt atom-decorated porous carbon matrix (Pt@PCM) electrocatalyst. Comparing with the commercial Pt/C-20% catalyst, the newly developed Pt@PCM hybrid delivers greatly improved mass activity (up to 25 times) for HER. XAFS analyses and DFT calculation confirm that the lattice confined Pt atoms should be the main contributor to the catalytic performance. Furthermore, the isolated Pt atoms can also activate surrounding C and N atoms and make them active in the hydrogen evolution process.

Ru possesses similar bonding strength with hydrogen to that of Pt, and performs as a cheaper alternative. However, fewer studies have been devoted to the Ru-based electrocatalysts for HER. Lou and co-workers have applied the defect-rich carbon matrix to stabilize the atomically dispersed Ru reactive centers (ECM@Ru) for HER (Figure 4e,f).^[71] The ECM@Ru catalyst with the Ru loading amount of 0.68 wt% delivers low overpotential (63 mV at 10 mA cm⁻²) and high mass activity. The mass activity of ECM@Ru is an order of magnitude higher than that of the commercial Pt/C-20% catalyst at the overpotential of 100 mV. The authors conclude that the defects surrounding the Ru centers can enhance the local electric field and accelerate the reaction kinetics of hydrogen evolution.

Developing precious-metal-free electrocatalysts for HER is also intensively explored. Chen and co-workers have developed a MOFs derived single W-atom catalyst (W-SAC) for efficient electrochemical HER.^[84] High-angle annular dark-field scanning transmission electron microscopy (HAADF-STEM) and XAFS spectroscopy investigations confirm that the W atoms are isolated with the favored coordination configuration of W₁N₁C₃. The overpotential of 85 mV is required for the W-SAC to give the current density of 10 mA cm⁻² in the alkaline solution, which is nearly

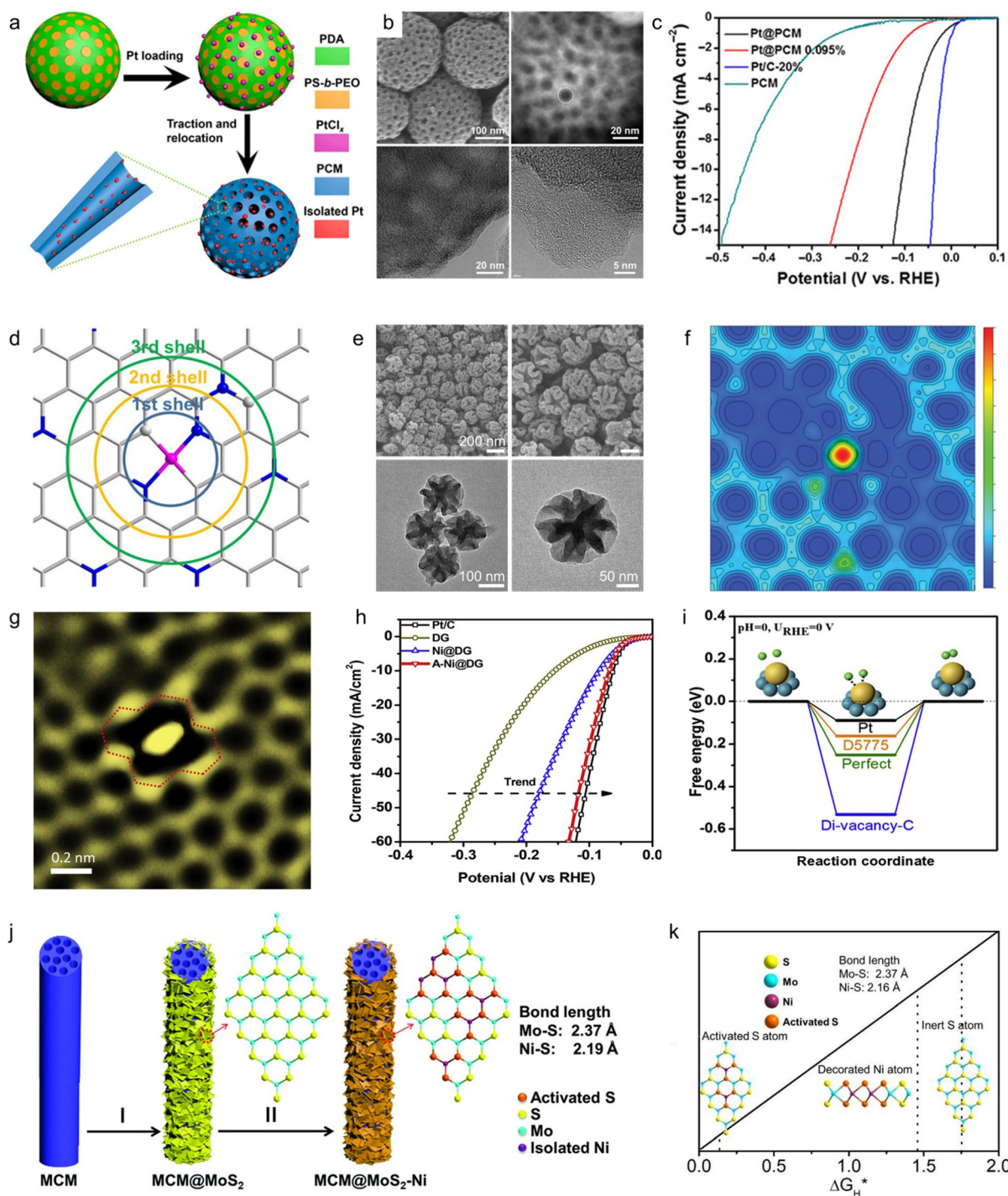


Figure 4. (a) Schematic description for the synthetic procedure of Pt@PCM. (b) Morphological characterizations for Pt@PCM. (c) Electrochemical hydrogen evolution curves of different catalysts. (d) Schematic illustration of the activation mechanism for the isolated Pt reactive center.^[61] Copyright 2018, American Chemical Society. (e) Morphological characterizations for ECM@Ru. (f) Calculated distribution of charge density for ECM@Ru.^[71] Copyright 2020, Wiley-VCH Verlag GmbH & Co. KGaA, Weinheim. (g) Schematic description for the defect stabilized Ni atoms in graphene. (h) HER polarization curves of the catalysts in H₂SO₄ media. (i) Energy profiles of the A-Ni@DG for HER. Copyright 2019 Elsevier B.V.^[85] (j) Schematic illustration of the synthetic process for MCM@MoS₂-Ni, and (k) theoretical calculations for the effects of Ni decoration on the HER activity of MoS₂.^[86] Copyright 2018 Wiley-VCH Verlag GmbH & Co. KGaA, Weinheim.

comparable to that of commercial Pt/C-20% catalyst. DFT calculation reveals that the unique W₁N₁C₃ configuration plays a crucial role in boosting the HER performance. Du et al. have reported the graphene defect captured Ni species

(A-Ni@DG) for electrocatalytic hydrogen evolution (Figure 4g-i).^[85] Atomically dispersed Ni atoms on the defects of graphene are constructed by the incipient wetness impregnation method. The as-synthesized hybrid delivers remarkable

electrocatalytic hydrogen evolution activity with an overpotential of 70 mV to reach the current density of 10 mA cm^{-2} .

The isolated transition metal atoms can also perform as the regulator to trigger the intrinsic catalytic activity of two-dimensional metal dichalcogenides. Zhang et al. have decorated isolated Ni atoms into the crystal lattice of hierarchical MoS_2 nanosheets via the surface modification strategy (Figure 4j,k).^[86] As the atomic radius of the Ni atom is much smaller than that of the Mo atom from the MoS_2 , coordination imbalance is created, producing much-shortened Ni–S bond length and distorted geometry over the basal plane of MoS_2 . The adsorption free energy for H species over the coordinated S atoms is significantly changed and the related hydrogen evolution kinetics is highly accelerated.

3.2. OER

OER is not only the rate-determining step for the electrochemical water splitting, but also a crucial process in some other energy conversion processes, including the CO_2RR and metal-air batteries.^[87] OER involves multiple electron transfer steps and always exhibits some intrinsically sluggish kinetics. This fact stimulates the exploration of efficient electrocatalysts with greatly boosted reaction kinetics. Precious metal-based catalysts (Ru and Ir) are the state-of-the-art electrocatalysts for OER, however, their widespread applications are also greatly hindered by the scarcity and high cost.^[88,89]

Cao and co-workers have decorated the isolated Ru centers into the N modified carbon matrix via a wet-chemical approach (Figure 5a–d).^[90] As demonstrated by the EXAFS analysis, the isolated Ru atoms are stabilized by four N atoms in the configuration of $\text{Ru}_1\text{-N}_4$ moieties. The as-synthesized hybrid delivers greatly improved mass activity for the oxygen evolution in acidic media, requiring an overpotential of 267 mV to reach the current density of 10 mA cm^{-2} . The authors believe that the reported catalyst is among the best OER electrocatalysts in acidic media. DFT calculations further suggest that the constructed O- $\text{Ru}_1\text{-N}_4$ sites possess much-reduced energy barrier for the O–O coupling in the reaction process.

Great endeavors have also been devoted to improving the activity of earth-abundant electrocatalysts for replacing the precious metal-based catalysts. For example, Lou and co-workers have developed a facile method for synthesizing Ni- N_4 units decorated hollow carbon matrix (HCM@Ni-N) for OER (Figure 5e–j).^[48] The correlation between the atomistic structure and electrocatalytic activity towards OER is also confirmed. XAFS analyses reveal that the isolated Ni atoms are stabilized by coordinated N atoms in the unsaturated configuration. The HCM@Ni-N delivers excellent performance and requires a small overpotential of 304 mV for achieving the OER current density of 10 mA cm^{-2} . The performance is much better than the samples with the sole Ni decoration or N modification, and even better than the commercial RuO_2 . The activity trend for the samples is consistent with the theoretically computed adsorption ener-

getics. The authors conclude that the effective electronic coupling between the Ni and N atoms results in the greatly accelerated OER kinetics.

4. SACs for electrocatalytic CO_2RR

Electrochemical CO_2 reduction into chemical products and renewable fuels represents a promising solution to mitigate the energy shortage and environmental challenges.^[91] However, due to the extremely inert C=O bond in the CO_2 molecule, the overpotential to initiate the reaction is rather high. Besides, the CO_2 reduction process has to compete with the HER in the liquid-phase reaction system. Thus, the low conversion efficiency and poor selectivity are the main bottlenecks for the real application of the electrochemical CO_2 reduction.^[92,93] It is therefore of high urgency to develop some low-cost electrocatalysts for driving the CO_2 reduction process with high efficiency and selectivity, but it is certainly very challenging.^[94]

SACs with maximized atomic efficiency and low-coordinated reactive centers exhibit remarkable performance in a variety of energy conversion processes.^[95,96] The homogeneously dispersed reactive centers and the uniform geometric configuration in SACs are favorable for the improvement of the catalytic selectivity. Moreover, such precise configurations render heterogeneous systems more convenient for investigating the underlying mechanisms of CO_2 reduction and developing more efficient catalysts. Thus, SACs offer great potentials for obtaining high selectivity and efficiency in the CO_2 reduction process.

4.1. CO_2RR to CO/HCOOH products

According to the more recent advances achieved, CO and HCOOH are the main products for the CO_2RR on SACs.^[92] This phenomenon can be attributed to the inherent characteristics of SACs. Firstly, as confirmed by the DFT calculations, the isolated reactive centers possess the appropriate adsorption energy for the intermediates such as CO^* and HCOO^* , which is in favor of the generation of the CO and HCOOH products. Moreover, due to the absence of metal ensembles in the SACs, the C–C couplings occurring over two adjacent active centers are always blocked over the isolated reactive centers.

Wang and co-workers have developed a facile approach for decorating the isolated Ni atoms onto the commercial carbon black (Figure 6a–d).^[74] The as-synthesized hybrid is further applied for electrochemical CO_2 reduction in the gas-phase electrocatalytic reactor. The single Ni atom catalyst delivers impressive performance for CO_2RR in the traditional H-cell. The CO Faradaic efficiency (FE) at -0.681 V versus reversible hydrogen electrode (vs. RHE) is confirmed as 99% in KHCO_3 aqueous electrolyte. Moreover, nearly 100% generation of CO is achieved under the high operation current density (larger than 100 mA cm^{-2}). The overall current can be further raised to 8 A in the up-scaling electrode ($10 \times 10 \text{ cm}^2$ per unit cell), while the exclusive CO

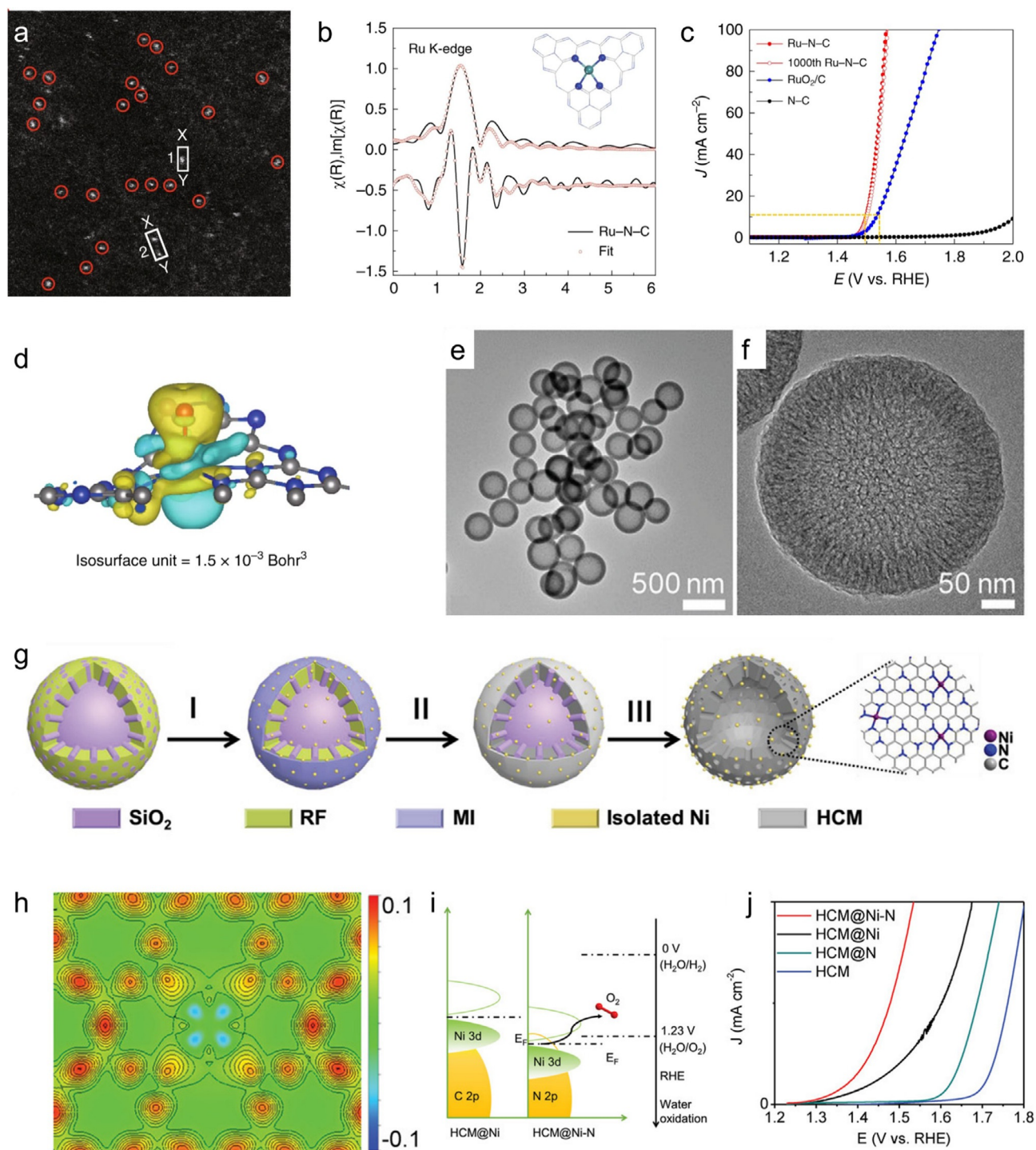


Figure 5. (a) HAADF-STEM image of Ru-N-C (b) The EXAFS curve of Ru-N-C (c) Electrocatalytic OER performances of the Ru-N-C and commercial RuO₂/C in 0.5 M H₂SO₄ electrolyte. (d) Differential charge density diagram of the O-Ru₁-N₄.^[90] Copyright 2019 Nature Publishing Group. (e,f) Morphological characterizations for HCM@Ni-N. (g) Schematic illustration for the synthesis of HCM@Ni-N. (h) Calculated charge density distribution of HCM@Ni-N. (i) Schematic band diagrams of HCM@Ni and HCM@Ni-N. (j) OER polarization curves of the electrocatalysts.^[48] Copyright 2019 Wiley-VCH Verlag GmbH & Co. KGaA, Weinheim.

evolution rate of 3.34 Lh⁻¹ per unit cell can be well maintained. Zhang and co-workers have constructed isolated Bi atoms decorated carbon matrix through thermal decomposition of a Bi-based MOF and dicyandiamide (Figure 6e).^[97] The catalyst delivers impressive activity for the

conversion of CO₂ to CO. High FE (97%) and turnover frequency (5535 h⁻¹) are confirmed at a low overpotential of 0.39 V versus reversible hydrogen electrode. Experimental results and DFT calculations verify that the Bi-N₄ units should be the real active centers for CO₂ activation, generating

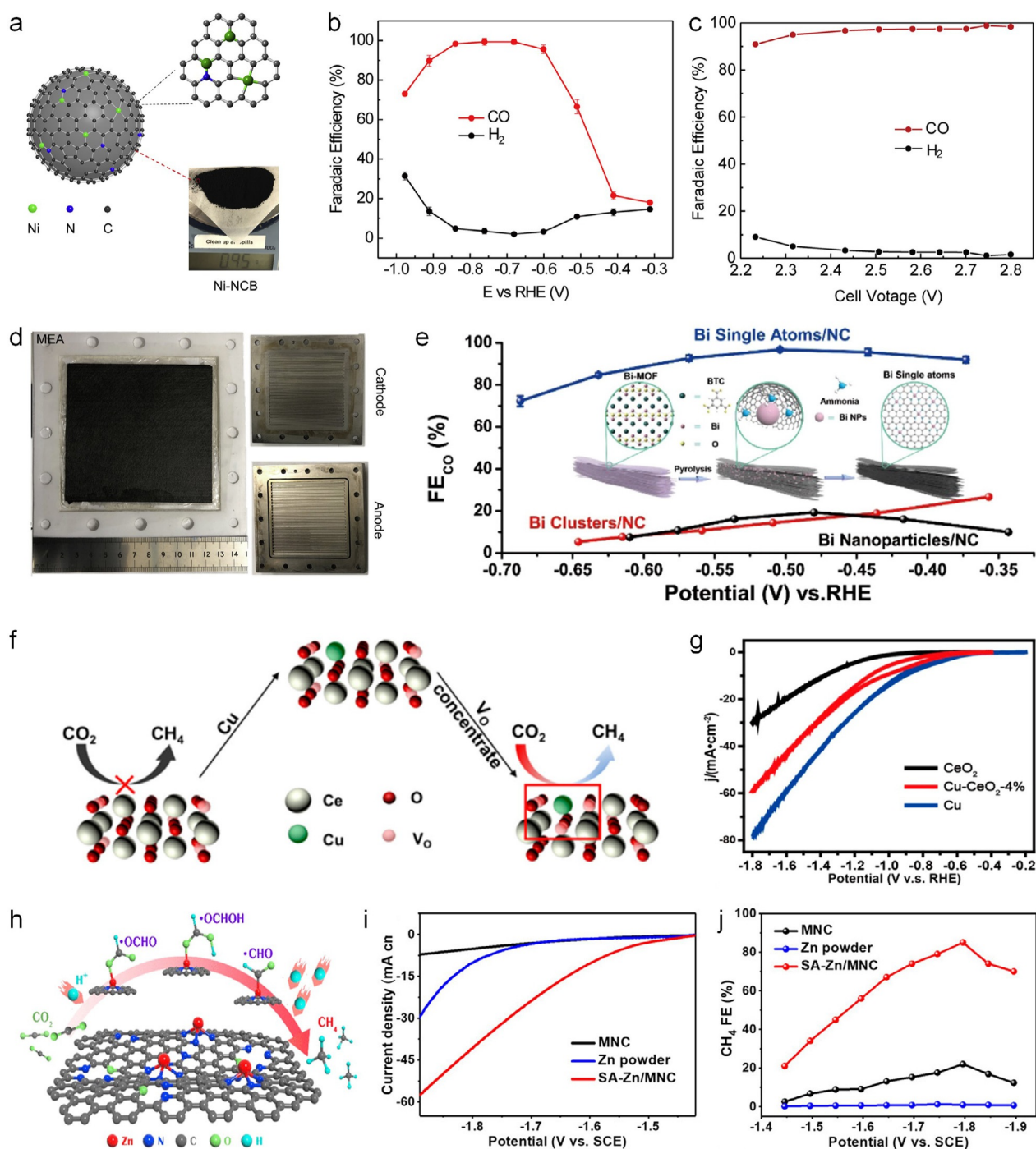


Figure 6. (a) Schematic description for the structure of Ni SACs. (b) FEs of H₂ and CO in H-cell. (c) FEs of H₂ and CO in the anion membrane electrode assembly. (d) Photographs of individual cell components in the membrane electrode assembly.^[124] Copyright 2019 Elsevier B.V. (e) Schematic for the construction of Bi-SACs from the Bi-MOF.^[97] Copyright 2019 American Chemical Society. (f) Schematic description for the role of the isolated Cu atoms in the CO₂ reduction process. (g) Linear sweep voltammetric curves for the CO₂ reduction with varied catalysts.^[100] Copyright 2018 American Chemical Society. (h) Schematic illustration of the evolution path of CH₄ over SA-Zn/MNC. (i) Linear sweep voltammetric curves for the CO₂ reduction of varied catalysts. (j) FEs for CH₄.^[101] Copyright 2020 American Chemical Society.

the key intermediate of HCOO* with a low free energy barrier.

Xie and co-workers have constructed exclusive Ni-N₄ centers via a topochemical transformation approach.^[98] Topochemical transformation by carbon layer coating guarantees the Ni-N₄ configuration to a maximized extent and averts the

growth of isolated Ni atoms to particles, offering abundant reactive centers for the CO₂ reduction. The Ni-N₄ catalyst delivers a maximized FE of 99% at -0.81 V vs. RHE for CO with a current density of 28.6 mA cm⁻². Moreover, the high FE (over 90%) can be well maintained in a wide potential window ranging from -0.5 to -0.9 V vs. RHE. Experimental

results and DFT calculation demonstrate that the Ni-N₄ reactive centers deliver greatly reduced energy barrier and improved charge transfer efficiency in the CO₂ reduction process, leading to boosted selectivity and activity for the conversion of CO₂ to CO.

As an intriguing liquid production of CO₂ electrocatalytic reduction, HCOOH has drawn broad interest in energy conversion and storage. Zu et al. have decorated the isolated Sn atoms onto the N modified carbon matrix for electrocatalytic CO₂ reduction. The hybrid can be synthesized in kilogram-scale by the quick freeze-vacuum drying-calcination method.^[99] HAADF-STEM and XAFS investigations confirm that the positively charged Sn atoms are atomically dispersed, which enables the CO₂ activation and protonation to proceed spontaneously. DFT calculation confirms that the positively charged Sn center is favorable for stabilizing the CO₂* and HCOO*, resulting in greatly accelerated reaction kinetics. This claim is also confirmed by the decreased desorption energy and the elongated bond length between Sn and HCOO⁻. As a result, a low onset overpotential (60 mV) for formate evolution and a large turnover frequency value (11930 h⁻¹) are observed in isolated Sn atoms decorated graphene.

4.2. CO₂RR to products beyond CO and HCOOH

Converting CO₂ into higher value-added products such as alcohols or hydrocarbons is more challenging and only a limited number of reports has emerged. As an example, Zheng and co-workers have decorated isolated Cu sites into CeO₂ with multiple oxygen vacancies and optimized the CO₂ electrocatalytic reduction to CH₄ (Figure 6 f,g).^[100] Structural characterizations indicate the isolated Cu centers are five coordinated with unsaturated configuration, demonstrating the direct association of oxygen vacancies for the isolated Cu centers. DFT calculations suggest that each isolated Cu center in CeO₂ (110) surface can stably enrich up to three oxygen vacancies, serving as the high-efficiency reactive center for CO₂ adsorption and activation. The authors attribute the excellent CH₄ selectivity to the existence of the multiple oxygen vacancies in CeO₂ framework surrounding the atomically dispersed Cu sites.

Xin and co-workers have decorated Zn species into the microporous N-doped carbon (Zn-SACs) by direct calcination of Zn based coordination polymer under high temperature (Figure 6 h-j).^[101] EXAFS investigations identify that the isolated Zn atoms are stabilized by surrounding N atoms. The as-synthesized electrocatalyst undergoes an eight-electron-transfer step and generates CH₄ in the CO₂RR process. It delivers remarkable catalytic performance with a high FE (85%) and a partial current density (-31.8 mA cm⁻²) at a potential of -1.8 V vs. saturated calomel electrode. Its high stability is also confirmed and no obvious current fluctuation or large FE drop is detected during the operation course of 35 hours. Theoretical calculation confirms that the O atom instead of the C atom in HCOO* prefers to coordinate with isolated Zn reactive centers in the reaction process, resulting

in the suppression for the generation of CO and thus promoting the evolution of CH₄.

He and co-workers have decorated the isolated Cu atoms into through-hole carbon nanofibers (CuSAs/TCNFs) for CO₂RR.^[102] The developed catalyst converts the CO₂ into nearly pure methanol with the FE of 44% at -0.9 V vs. RHE in liquid phase. The partial current density for methanol evolution is confirmed as -93 mA cm⁻². The self-supporting and through-hole architecture of CuSAs/TCNFs realizes the exposure of isolated Cu centers to the largest extent, and greatly boosts the reduction efficiency for the hybrid. DFT calculations reveal that the isolated Cu reactive centers possess a rather high binding energy for the CO* intermediate. Therefore, CO* could be further reduced to methanol, instead of being easily released as CO from the catalyst surface.

5. Operando monitoring the structural evolution in catalysis

The relationship between the structure and performance has long been pursued as a key fundamental issue in heterogeneous catalysis. However, it is still blurry for a majority of reaction systems. Operando characterizations are powerful techniques for providing fundamental structural evolution information about the structure-performance relationships under diverse catalytic processes.^[103-106] However, one of the major challenges for further exploring the nature of active sites and reaction mechanisms is the development of model catalysts.^[107] The obstacles not only lie in the complicated interaction between the reactant and reactive sites, but also arise from the non-uniform distribution of the reactive centers and the structural diversity of the catalysts.^[108] For the particle-based catalyst, the size and shape of the particles and the mutual interaction between the particle and the support are crucial parameters for the catalytic performance. It is challenging to disentangle the less important parameters from those interplaying factors and rationalize the precise relationship between the structure and performance.^[109-111] Fortunately, SACs with uniformly dispersed reactive centers in nearly identical configuration provide us an elegant platform for identifying the nature of the reactive centers by monitoring the dynamic structural evolution of active sites during catalytic process at atomic level.^[43,112] The obtained information is important for studying catalytic mechanism as well as the underlying structure-performance relationship.

5.1. Operando XAFS

Operando XAFS characterization techniques have been quickly developed in the past years. It generally includes the XANES and EXAFS spectra.^[113] The XANES spectrum mainly provides information about electronic structure and chemical valence state of the detected metal center, while the EXAFS spectrum reflects the coordination geometry, the bonding length and the true atomic spatial distribution of the reactive centers.^[114] By constructing the operando XAFS

based reaction setup, the structural evolution in terms of chemical states, coordination conditions of the reactive centers can be well monitored and analyzed.

Li and co-workers have decorated isolated Co atoms into the Ru nanosheet for efficient hydrogen evolution (Fig-

ure 7a,b).^[115] Structural evolutions of the Co and Ru in the hybrids are monitored by operando XAFS measurements during the catalytic process. No obvious change is detected in the operando Co/Ru K-edge EXAFS and XANES spectra under varied operating conditions. These results not only

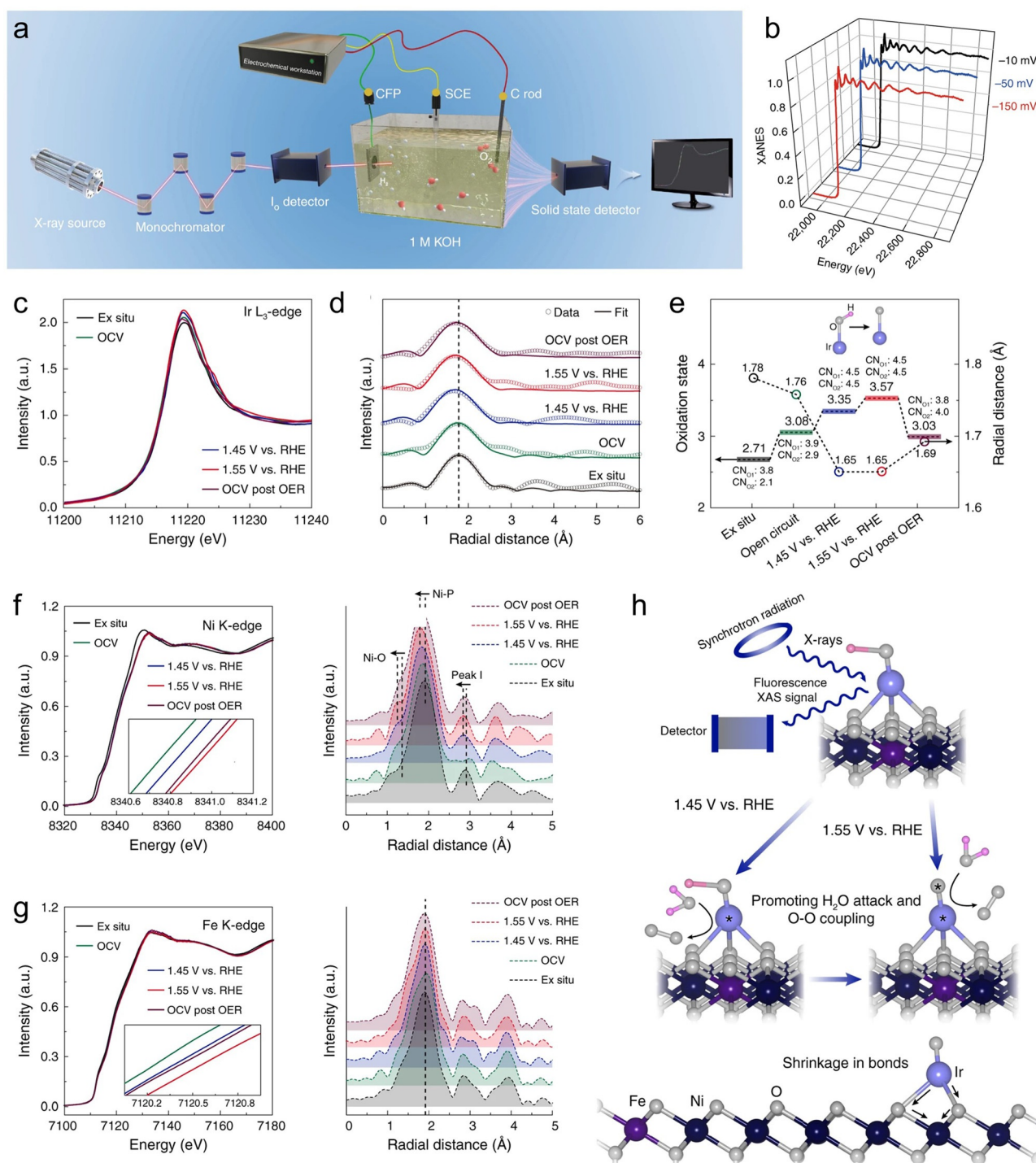


Figure 7. (a) Schematic illustration of operando XAFS measurements for Co-substituted Ru. (b) Ru K-edge XANES spectra of Co-substituted Ru.^[115] Copyright 2018 Nature Publishing Group. (c) Operando XANES spectra of np-Ir/NiFeO. (d) EXAFS spectra of np-Ir/NiFeO for Ni-O bonding fitting. (e) The oxidation states obtained from the absorption edge fitting. (f) Ni K-edge XANES spectra of np-Ir/NiFeO recorded at operando investigations under different potentials. (g) Fe K-edge XANES spectra of np-Ir/NiFeO recorded at operando investigations under different potentials. (h) Schematic description for the OER mechanism obtained from the operando XAFS investigations.^[116] Copyright 2020 Nature Publishing Group.

suggest the high stability of the local coordination sphere of Co-substituted Ru catalyst, but also demonstrate the structural evolution for the reactive centers is a quick and successive process.

Tan and co-workers have utilized a self-reconstruction strategy to construct isolated Ir decorated oxyhydroxides (Ir/NiFeO) for efficient OER (Figure 7c–h).^[116] The structural evolution of the isolated Ir atoms is monitored during the OER process. Operando XAFS investigations indicate that no obvious change for the EXAFS spectrum is detected with the increase of anodic potential. This result indicates that the coordination number for the isolated Ir center is very stable in the catalytic process. However, the white line intensity of the XANES spectrum increases obviously during electrochemical oxygen evolution process, indicating the generation of Ir species in a higher oxidation state. As there is no obvious change for the coordination number of the Ir centers, the increase for the oxidation state of Ir centers under higher anodic potential should not be ascribed to the chemisorption of the intermediate species. The authors thus propose the occurring of deprotonation process (Ir-OH to Ir-O*) over Ir sites during OER. The deprotonation step renders the variation for the oxidation state of the reactive centers while casts no influence on the coordination number of the local geometry. The generation of the active oxygen species is thus realized in the deprotonation step, which is fundamental for oxygen evolution.

Liu and co-workers have developed the atomically distributed nickel on nitrogenized graphene (A-Ni-NG) as an efficient catalyst for electrochemical CO₂ reduction.^[117] Operando XAFS investigations are conducted for monitoring the CO₂ reduction process. Comparing with the spectrum of A-Ni-NG sample in Ar-saturated KHCO₃ solution under open-circuit voltage bias, an obvious shift (about 0.4 eV) for the Ni K-edge XANES spectrum is observed in CO₂-saturated KHCO₃ solution, demonstrating the increase for the oxidation state of the reactive centers. The authors conclude that the delocalized electron in the 3d_{x²-y²} orbital and effective charge transfer from reactive centers to the adsorbed CO₂ molecule should be the main reasons for these variations. The Ni K-edge XANES spectra of A-Ni-NG shift back to lower energy in the reduction process, confirming the recovery of low-oxidation-state Ni and the release of the products. The slight increase for the main peak intensity in the EXAFS spectrum is also detected during the CO₂ reduction process, which should be attributed to the coordination between the isolated Ni sites and the intermediates. Besides, a peak shift of about 0.04 Å in Fourier transform curves of Ni K-edge EXAFS spectrum is also observed for the A-Ni-NG under the operation potential of -0.7 V, confirming that the bond length of Ni-N expands during catalysis. The authors also believe that the redistribution of the electrons in the Ni 3d orbital during the CO₂ reduction process results in the distortion of the Ni atoms out of the graphene plane, and the monovalent Ni(i) site with a d⁹ electronic configuration should be the real reactive center for the CO₂ reduction.

5.2. Operando Fourier transform infrared (FTIR) spectroscopy

Operando FTIR technique is highly sensitive to the vibration mode of the adsorbed molecules (reactants or products) on active sites, and can thus provide decisive evidences to track the reaction pathways in single-atom catalysis.^[39,118] Its absorption peak position can always be used for revealing the structural composition or confirming the chemical groups present. In addition, the content of chemical groups can be quantitatively analyzed by the absorption intensity of FTIR.^[119] Compared with operando XAFS, operando FTIR spectroscopy is more focused on the detection of catalytic reaction intermediates with fast characterization speed and high sensitivity.^[120]

Liu and co-workers have constructed the hetero pyridinic- and amino-N ligands coordinated single Co atom catalyst (HNC-Co) for OER in the acidic environment (Figure 8a–e).^[121] Operando FTIR investigation is conducted under realistic OER working conditions for obtaining further comprehension of the catalytic oxygen evolution mechanism over the HNC-Co catalyst. It is worthy to note that a new absorption band assigned to the key O* intermediate over the Co reactive centers is observed at about 1248 cm⁻¹ under the operation potential of 1.38 V. With the removal of the operation potential, the new vibrational band totally vanishes. These observations may indicate that the coordination between the O* intermediate and the isolated Co site in HNC-Co is detected in the oxygen evolution process. This conclusion is further confirmed by Yao and colleagues, who have decorated the Ru₁-N₄ sites into nitrogen-carbon support (Ru-N-C) and applied the as-synthesized hybrid for OER under acidic condition.^[90] When conducting the reaction at the operation potential of 1.5 V, a new obvious absorption band is observed, revealing the existence of an essential intermediate in the OER process. The new absorption band gradually disappears with the decrease in the applied potential. This vibrational absorption band is confirmed as single oxygen adsorption over the Ru-N₄ site, resulting from the generation of the intermediate species during the reaction.

The adsorbed water molecules at the solid-liquid electrochemical interfaces can also be monitored by the operando FTIR investigation. Su and co-workers have investigated the structural evolution of reactive centers for oxygen reduction at the solid-liquid electrochemical interface.^[122] Related transformations of reactive intermediates are also detected over a single-atom Ni catalyst (Ni₁-NC) (Figure 8f–j). As confirmed by the operando FTIR results, the intensities for the absorption band at 908 cm⁻¹ increase with the decrease of the operation potential, indicating the generation of a crucial intermediate over Ni₁-NC during the oxygen reduction process. Besides, the new absorption band appearing at about 3465 cm⁻¹ should be ascribed to the stretching mode of the hydroxyl radicals (OH*), indicating the adsorption of water molecules over the reactive sites. The band intensity for the adsorbed OH* increases quickly with the decrease of the applied potential. The authors conclude that the adsorbed OH* species may locate at the N/C sites that surround the

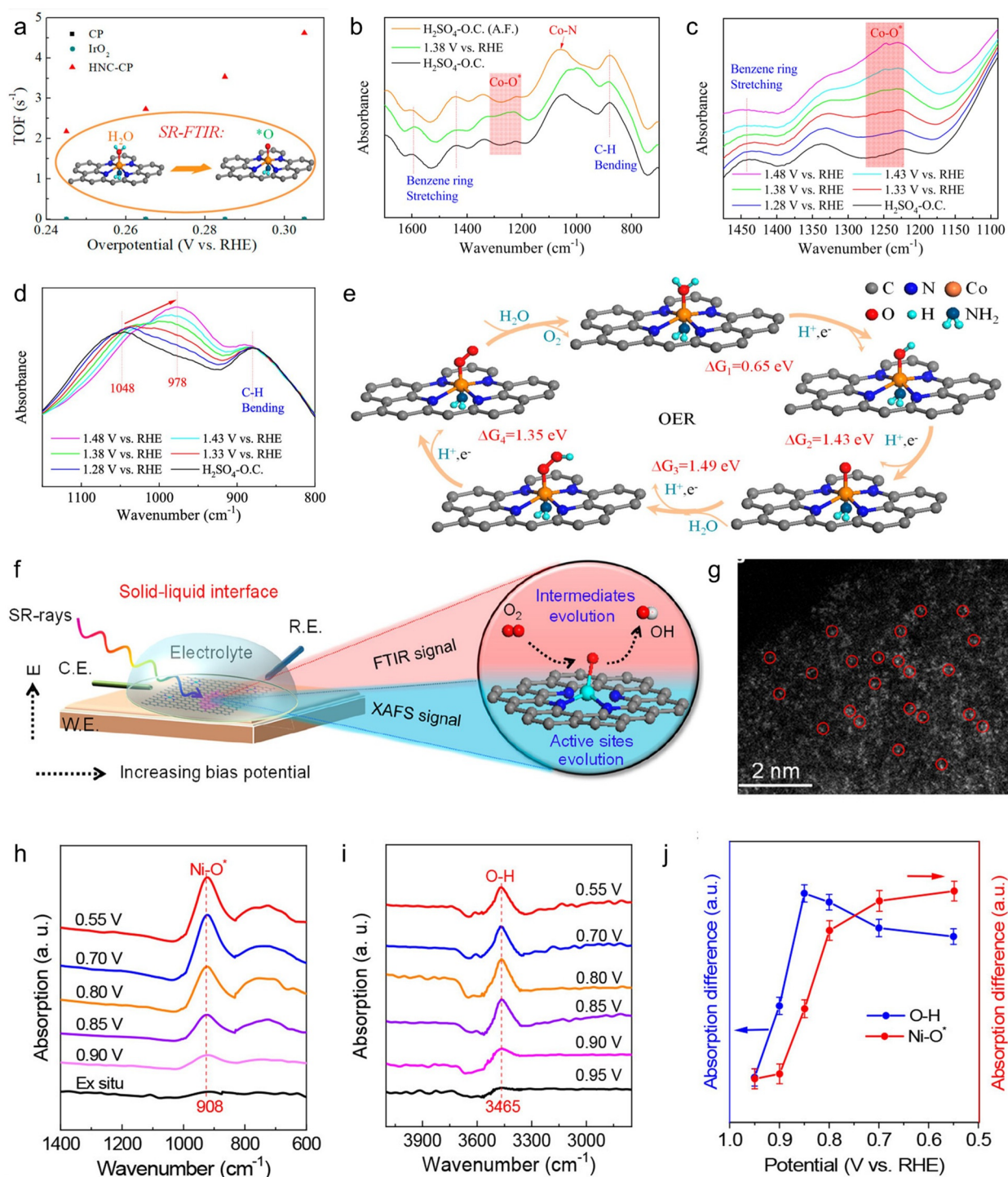


Figure 8. (a) Turnover frequencies of catalysts at different potentials. (b) Operando FTIR investigations for HNC-Co. (c,d) FTIR signal in the ranges of 1100–1500 cm⁻¹ (c) and 800–1200 cm⁻¹ (d) under various potentials for OER. (e) Proposed mechanism for the oxygen evolution of HNC-Co.^[121] Copyright 2019 American Chemical Society. (f) Schematic description for the operando characterization for the Ni₁-NC electrocatalyst. (g) HAADF-STEM image of Ni₁-NC. (h,i) Operando FTIR investigation in different detection ranges. (j) Infrared signals at 908 and 3465 cm⁻¹ versus the potentials for Ni₁-NC.^[122] Copyright 2020 American Chemical Society.

isolated Ni sites and thus devote to the generation of the essential O* intermediates during the catalytic process.

6. Conclusions and prospects

With unparalleled geometric and electronic structures, SACs have undergone great progresses in the past ten years and delivered fascinating performance in heterogeneous

catalysis. SACs have also provided an elegant platform for bridging the homogeneous and heterogeneous catalysis by offering the homogeneously dispersed reactive centers over heterogeneous supports. Our comprehensions of SACs have been rapidly developed from the aspects of catalyst construction, characterization, performance evaluation, and mechanistic interpretation. However, despite the initial success obtained, there exist many challenges in the development and application of SACs. Some future perspectives, research directions, and possible solutions for addressing the existing challenges are elaborated as below:

- 1) Improving the loading contents of the isolated reactive centers of SACs is crucial to meet the requirements of real applications for heterogeneous catalysis, and is also one major challenge for the development of SACs. Thus, increasing the number of anchor sites and boosting the anchoring capability by strengthening the metal-support interaction are highly desirable for the construction of SACs. In addition, designing SACs with a particular configuration represents an efficient strategy to optimize and improve the catalytic performance of SACs. The modular strategy for constructing SACs can guarantee the basic geometry of the reactive centers and is thus highly recommended.^[27] Furthermore, machine learning based design strategies become a new trend and might offer some guidelines for synthesizing catalyst with high efficiency, and should also be introduced with care in the production of SACs in large scale.^[123]
- 2) Research towards regulating the coordination sphere of SACs is still in its early stage. Modifying the first coordination sphere of the reactive centers with heteroatoms holds great promise for further exploring the intrinsic activity of the reactive centers. Besides, adjusting the coordination numbers of the reactive centers also represents an elegant approach for modulating the catalytic performances. As many catalytic reactions involve complicated multistep reaction processes, the coordination sphere is an important factor for activating the intermediates. The electronic coupling between the isolated centers and coordinated atoms, as well as the related catalytic activation of nonmetallic atoms, should be emphasized in future research.
- 3) In the past years, characterization technologies for SAC have also undergone rapid development, which can provide more detailed information for the overall structure of the SACs. The existence of the defects in the supports has been precisely characterized and the generation of new defects with the introduction of the isolated active centers is under intensive investigations. However, there are still many challenges in controlling the amount of defects and quantifying defects and the related positive effects on SACs. Thus, it is of vital importance to quantify these defects by using combined technologies and establish the relationship between the catalytic performances and the defects existed. Moreover, tracking the evolution of defects and conducting real-time observation for defects under the reaction conditions are very helpful for figuring out the strong electronic coupling between defects and the isolated reactive centers and a deeper understanding on the nature of SACs. Lastly, the contribution of defects for the catalytic performance should be recognized and quantified if possible, and it is likely that some defects can even serve as the real active centers.
- 4) Although tremendous attention has been devoted to the development of SACs, only a few reports are related to the construction of di-nuclear and multi-nuclear species decorated on the heterogeneous supports. The gap between well-established particle-based catalysts and SACs is still very obvious. The recently developed atom by atom strategy for constructing the atomically precise metal clusters holds great promise for bridging the SACs and particle-based catalysts.^[57] With the development of this sub-field, the new concept of single-cluster catalysts has emerged and should be developed as a new research frontier in heterogeneous catalysis. Although SACs represent the maximized atomic utilization, it does not necessarily mean the optimized catalytic performance for particular reaction types. Sub-clusters with the size below 1 nm are also characterized by the high atomic utilization and strong quantum effect.^[4] Research along this direction will offer new comprehension on the structure–activity correlations. The achievements would certainly benefit the whole heterogeneous catalysis community.
- 5) Although intensive studies have been conducted for exploring energy conversions, more attention should be devoted to expanding the application of SACs in even broader areas, especially for those important industrial conversion processes. Fe and Co nanoparticles are widely applied for the Fischer–Tropsch synthesis in thermocatalysis. However, the application of SACs in this area is rather limited. Isolated Co or Fe centers might provide higher selectivity and activity in the Fischer–Tropsch reaction. Besides, Pt particles decorated zeolites have been proved as efficient catalysts for heavy oil hydrocracking. Pt-based SACs or isolated clusters should be developed and evaluated for the application of hydrocracking.
- 6) The synergetic effects of experimental investigations and DFT calculations greatly advance the development of catalysis. Generally, the theoretical calculations are conducted within the concept of potential energy surface, in which the simplified structural models are considered under idealized conditions in a stationary state. With the rapid development of computational technology, the simulation for the particular reaction types with more precise structural models under realistic conditions should be made available, which will provide more comprehensive understanding on the structural nature and related reaction mechanism. Moreover, the progress in the data science makes the application of big data strategies for discovering the underlying structure–performance relationships possible, which provides us great chances to predict the catalytic performances for screened materials and finally affords an elegant platform for designing and developing new catalysts.
- 7) As demonstrated by recent studies, operando XAFS and FTIR techniques have been performed as powerful tools

for monitoring the evolution of reactive centers at molecular level. The obtained results emphasize the complexity of the mechanisms for various catalytic reactions. However, all these progresses are still far from the full comprehension of the nature of reactive centers. Many energy conversion processes involve multi-step reactions with unidentified reactive intermediates, unclear real active centers and unconfirmed reaction mechanisms, which greatly hinder our overall comprehension of the SACs and the energy conversion process. Thus, integrated operando characterization technologies with special reaction cells are urgently needed towards the comprehensive understanding of the reaction and revealing the nature of reactive centers. For example, combining the XAFS technology with the X-ray photoelectron spectroscopy and Raman techniques in the operando investigations may gain more comprehensive clues for the structural evolution, which are highly related to the coordination geometry, oxidation state and related reaction intermediates.

Acknowledgements

X.W.L. acknowledges the funding support from the Ministry of Education of Singapore through the Academic Research Fund (AcRF) Tier-2 grant (MOE2017-T2-2-003) and Tier-1 grant (RG116/18), and the National Research Foundation (NRF) of Singapore via the NRF Investigatorship (NRF-NRFI2016-04).

Conflict of interest

The authors declare no conflict of interest.

- [1] Y. Yang, Y. Qian, H. Li, Z. Zhang, Y. Mu, D. Do, B. Zhou, J. Dong, W. Yan, Y. Qin, *Sci. Adv.* **2020**, 6, eaba6586.
- [2] Y. Jiao, Y. Zheng, M. Jaroniec, S. Z. Qiao, *Chem. Soc. Rev.* **2015**, 44, 2060.
- [3] M. P. Browne, Z. Sofer, M. Pumera, *Energy Environ. Sci.* **2019**, 12, 41.
- [4] H. Zhang, P. Zhang, M. Qiu, J. Dong, Y. Zhang, X. W. Lou, *Adv. Mater.* **2019**, 31, 1804883.
- [5] S. Wang, B. Y. Guan, X. W. Lou, *J. Am. Chem. Soc.* **2018**, 140, 5037.
- [6] S. Sorcar, Y. Hwang, J. Lee, H. Kim, K. M. Grimes, C. A. Grimes, J. W. Jung, C. H. Cho, T. Majima, M. R. Hoffmann, *Energy Environ. Sci.* **2019**, 12, 2685.
- [7] N. Lazouski, M. Chung, K. Williams, M. L. Gala, K. Manthiram, *Nat. Catal.* **2020**, 3, 463.
- [8] H. Zhang, S. Zuo, M. Qiu, S. Wang, Y. Zhang, J. Zhang, X. W. Lou, *Sci. Adv.* **2020**, 6, eabb9823.
- [9] H. Zhang, T. Wang, J. Wang, H. Liu, T. D. Dao, M. Li, G. Liu, X. Meng, K. Chang, L. Shi, *Adv. Mater.* **2016**, 28, 3703.
- [10] G. Xu, H. Zhang, J. Wei, H. Zhang, X. Wu, Y. Li, C. Li, J. Zhang, J. Ye, *ACS Nano* **2018**, 12, 5333.
- [11] Y. Fu, Y. Shan, G. Zhou, L. Long, L. Wang, K. Yin, J. Guo, J. Shen, L. Liu, X. Wu, *Joule* **2019**, 3, 2955.
- [12] Y. Zang, S. Niu, Y. Wu, X. Zheng, J. Cai, J. Ye, Y. Xie, Y. Liu, J. Zhou, J. Zhu, *Nat. Commun.* **2019**, 10, 1217.
- [13] M. Liu, M. Liu, X. Wang, S. M. Kozlov, Z. Cao, P. De Luna, H. Li, X. Qiu, K. Liu, J. Hu, *Joule* **2019**, 3, 1703.
- [14] H. Zhang, G. Liu, L. Shi, H. Liu, T. Wang, J. Ye, *Nano Energy* **2016**, 22, 149.
- [15] B. A. Zhang, T. Ozel, J. S. Elias, C. Costentin, D. G. Nocera, *ACS Cent. Sci.* **2019**, 5, 1097.
- [16] D. Jeon, J. Park, C. Shin, H. Kim, J.-W. Jang, D. W. Lee, J. Ryu, *Sci. Adv.* **2020**, 6, eaaz3944.
- [17] G. Liu, P. Li, G. Zhao, X. Wang, J. Kong, H. Liu, H. Zhang, K. Chang, X. Meng, T. Kako, *J. Am. Chem. Soc.* **2016**, 138, 9128.
- [18] Y. Li, R. Zhang, W. Zhou, X. Wu, H. Zhang, J. Zhang, *ACS Nano* **2019**, 13, 5533.
- [19] X. Wu, J. Dong, M. Qiu, Y. Li, Y. Zhang, H. Zhang, J. Zhang, *Nanoscale Horiz.* **2020**, 5, 359.
- [20] H. Zhang, W. Zhou, J. Dong, X. F. Lu, X. W. Lou, *Energy Environ. Sci.* **2019**, 12, 3348.
- [21] H. Zhang, Z. Ma, J. Duan, H. Liu, G. Liu, T. Wang, K. Chang, M. Li, L. Shi, X. Meng, *ACS Nano* **2016**, 10, 684.
- [22] Z. W. Seh, J. Kibsgaard, C. F. Dickens, I. Chorkendorff, J. K. Nørskov, T. F. Jaramillo, *Science* **2017**, 355, 6321.
- [23] L. Liu, A. Corma, *Chem. Rev.* **2018**, 118, 4981.
- [24] H. Zhang, J. Nai, L. Yu, X. W. Lou, *Joule* **2017**, 1, 77.
- [25] S. Anantharaj, S. Kundu, *ACS Energy Lett.* **2019**, 4, 1260.
- [26] H. Zhang, G. Liu, L. Shi, J. Ye, *Adv. Energy Mater.* **2018**, 8, 1701343.
- [27] H. Zhang, W. Zhou, T. Chen, B. Y. Guan, Z. Li, X. W. Lou, *Energy Environ. Sci.* **2018**, 11, 1980.
- [28] X. Li, X. Yang, Y. Huang, T. Zhang, B. Liu, *Adv. Mater.* **2019**, 31, 1902031.
- [29] C. Gao, J. Low, R. Long, T. Kong, J. Zhu, Y. Xiong, *Chem. Rev.* **2020**, 120, 12175.
- [30] Q. Zhang, J. Guan, *Adv. Funct. Mater.* **2020**, 30, 2000768.
- [31] X. Wu, H. Zhang, J. Dong, M. Qiu, J. Kong, Y. Zhang, Y. Li, G. Xu, J. Zhang, J. Ye, *Nano Energy* **2018**, 45, 109.
- [32] C. Lu, R. Fang, X. Chen, *Adv. Mater.* **2020**, 32, 1906548.
- [33] H. Zhang, X. F. Lu, Z.-P. Wu, X. W. Lou, *ACS Cent. Sci.* **2020**, 6, 1288.
- [34] X. Cui, W. Li, P. Ryabchuk, K. Junge, M. Beller, *Nat. Catal.* **2018**, 1, 385.
- [35] Y. Zhu, J. Sokolowski, X. Song, Y. He, Y. Mei, G. Wu, *Adv. Energy Mater.* **2020**, 10, 1902844.
- [36] R. T. Hannagan, G. Giannakakis, M. Flytzani-Stephanopoulos, E. C. H. Sykes, *Chem. Rev.* **2020**, 120, 12044.
- [37] X. Li, L. Liu, X. Ren, J. Gao, Y. Huang, B. Liu, *Sci. Adv.* **2020**, 6, eabb6833.
- [38] L. Bai, C.-S. Hsu, D. T. Alexander, H. M. Chen, X. Hu, *J. Am. Chem. Soc.* **2019**, 141, 14190.
- [39] X. Li, X. Yang, J. Zhang, Y. Huang, B. Liu, *ACS Catal.* **2019**, 9, 2521.
- [40] E. Fabbri, D. F. Abbott, M. Nachttegaal, T. J. Schmidt, *Curr. Opin. Electrochem.* **2017**, 5, 20.
- [41] Y. Chen, S. Ji, C. Chen, Q. Peng, D. Wang, Y. Li, *Joule* **2018**, 2, 1242.
- [42] R. Lang, W. Xi, J.-C. Liu, Y.-T. Cui, T. Li, A. F. Lee, F. Chen, Y. Chen, L. Li, L. Li, *Nat. Commun.* **2019**, 10, 234.
- [43] A. Wang, J. Li, T. Zhang, *Nat. Rev. Chem.* **2018**, 2, 65.
- [44] N. Daelman, M. Capdevila-Cortada, N. López, *Nat. Mater.* **2019**, 18, 1215.
- [45] H. Xu, D. Cheng, D. Cao, X. C. Zeng, *Nat. Catal.* **2018**, 1, 339.
- [46] X. Wang, Z. Chen, X. Zhao, T. Yao, W. Chen, R. You, C. Zhao, G. Wu, J. Wang, W. Huang, *Angew. Chem. Int. Ed.* **2018**, 57, 1944; *Angew. Chem.* **2018**, 130, 1962.
- [47] Y. Ren, Y. Tang, L. Zhang, X. Liu, L. Li, S. Miao, D. S. Su, A. Wang, J. Li, T. Zhang, *Nat. Commun.* **2019**, 10, 4500.
- [48] H. Zhang, Y. Liu, T. Chen, J. Zhang, J. Zhang, X. W. Lou, *Adv. Mater.* **2019**, 31, 1904548.

- [49] Y. Han, Y. Wang, R. Xu, W. Chen, L. Zheng, A. Han, Y. Zhu, J. Zhang, H. Zhang, J. Luo, *Energy Environ. Sci.* **2018**, *11*, 2348.
- [50] J. Han, P. An, S. Liu, X. Zhang, D. Wang, Y. Yuan, J. Guo, X. Qiu, K. Hou, L. Shi, Y. Zhang, S. Zhao, C. Long, Z. Tang, *Angew. Chem. Int. Ed.* **2019**, *58*, 12711; *Angew. Chem.* **2019**, *131*, 12841.
- [51] X. Long, Z. Li, G. Gao, P. Sun, J. Wang, B. Zhang, J. Zhong, Z. Jiang, F. Li, *Nat. Commun.* **2020**, *11*, 4074.
- [52] J. Zhang, Y. Zhao, C. Chen, Y.-C. Huang, C.-L. Dong, C.-J. Chen, R.-S. Liu, C. Wang, K. Yan, Y. Li, G. Wang, *J. Am. Chem. Soc.* **2019**, *141*, 20118.
- [53] Y. Chen, S. Ji, S. Zhao, W. Chen, J. Dong, W.-C. Cheong, R. Shen, X. Wen, L. Zheng, A. I. Rykov, *Nat. Commun.* **2018**, *9*, 5422.
- [54] Y. Mun, S. Lee, K. Kim, S. Kim, S. Lee, J. W. Han, J. Lee, *J. Am. Chem. Soc.* **2019**, *141*, 6254.
- [55] Z. Jiang, W. Sun, H. Shang, W. Chen, T. Sun, H. Li, J. Dong, J. Zhou, Z. Li, Y. Wang, *Energy Environ. Sci.* **2019**, *12*, 3508.
- [56] H. Li, L. Wang, Y. Dai, Z. Pu, Z. Lao, Y. Chen, M. Wang, X. Zheng, J. Zhu, W. Zhang, *Nat. Nanotechnol.* **2018**, *13*, 411.
- [57] H. Yan, Y. Lin, H. Wu, W. Zhang, Z. Sun, H. Cheng, W. Liu, C. Wang, J. Li, X. Huang, *Nat. Commun.* **2017**, *8*, 1070.
- [58] H. Xiang, W. Feng, Y. Chen, *Adv. Mater.* **2020**, *32*, 1905994.
- [59] M. Zhao, H.-B. Wang, L. N. Ji, Z. W. Mao, *Chem. Soc. Rev.* **2013**, *42*, 8360.
- [60] Y. Liu, Z. Li, Q. Yu, Y. Chen, Z. Chai, G. Zhao, S. Liu, W.-C. Cheong, Y. Pan, Q. Zhang, L. Gu, L. Zheng, Y. Wang, Y. Lu, D. Wang, C. Chen, Q. Peng, Y. Liu, L. Liu, J. Chen, Y. Li, *J. Am. Chem. Soc.* **2019**, *141*, 9305.
- [61] H. Zhang, P. An, W. Zhou, B. Y. Guan, P. Zhang, J. Dong, X. W. Lou, *Sci. Adv.* **2018**, *4*, eaao6657.
- [62] X. He, Q. He, Y. Deng, M. Peng, H. Chen, Y. Zhang, S. Yao, M. Zhang, D. Xiao, D. Ma, *Nat. Commun.* **2019**, *10*, 3663.
- [63] L. Liu, N. Wang, C. Zhu, X. Liu, Y. Zhu, P. Guo, L. Alfifil, X. Dong, D. Zhang, Y. Han, *Angew. Chem. Int. Ed.* **2020**, *59*, 819; *Angew. Chem.* **2020**, *132*, 829.
- [64] H. Zhang, J. Wei, J. Dong, G. Liu, L. Shi, P. An, G. Zhao, J. Kong, X. Wang, X. Meng, *Angew. Chem.* **2016**, *55*, 14310; *Angew. Chem.* **2016**, *128*, 14522.
- [65] X. Guo, G. Fang, G. Li, H. Ma, H. Fan, L. Yu, C. Ma, X. Wu, D. Deng, M. Wei, *Science* **2014**, *344*, 616.
- [66] Y. Zhang, L. Guo, L. Tao, Y. Lu, S. Wang, *Small Methods* **2019**, *3*, 1800406.
- [67] X. Rong, H. J. Wang, X. L. Lu, R. Si, T. B. Lu, *Angew. Chem. Int. Ed.* **2020**, *59*, 1961; *Angew. Chem.* **2020**, *132*, 1977.
- [68] Y. Jia, L. Zhang, A. Du, G. Gao, J. Chen, X. Yan, C. L. Brown, X. Yao, *Adv. Mater.* **2016**, *28*, 9532.
- [69] D. Yan, Y. Li, J. Huo, R. Chen, L. Dai, S. Wang, *Adv. Mater.* **2017**, *29*, 1606459.
- [70] J. Chen, S. K. Iyemperumal, T. Fenton, A. Carl, R. Grimm, G. Li, N. A. Deskins, *ACS Catal.* **2018**, *8*, 10464.
- [71] H. Zhang, W. Zhou, X. F. Lu, T. Chen, X. W. Lou, *Adv. Energy Mater.* **2020**, *10*, 2000882.
- [72] J. Zhang, X. Wu, W.-C. Cheong, W. Chen, R. Lin, J. Li, L. Zheng, W. Yan, L. Gu, C. Chen, *Nat. Commun.* **2018**, *9*, 1002.
- [73] S. Wei, A. Li, J.-C. Liu, Z. Li, W. Chen, Y. Gong, Q. Zhang, W.-C. Cheong, Y. Wang, L. Zheng, *Nat. Nanotechnol.* **2018**, *13*, 856.
- [74] D. Zhao, Z. Chen, W. Yang, S. Liu, X. Zhang, Y. Yu, W.-C. Cheong, L. Zheng, F. Ren, G. Ying, *J. Am. Chem. Soc.* **2019**, *141*, 4086.
- [75] J. Wang, Y. Gao, H. Kong, J. Kim, S. Choi, F. Ciucci, Y. Hao, S. Yang, Z. Shao, J. Lim, *Chem. Soc. Rev.* **2020**, *49*, 9154–9196.
- [76] B. You, Y. Sun, *Acc. Chem. Res.* **2018**, *51*, 1571.
- [77] M. Kim, J. Park, M. Kang, J. Y. Kim, S. W. Lee, *ACS Cent. Sci.* **2020**, *6*, 880.
- [78] D. Zhang, H. Zhao, B. Huang, B. Li, H. Li, Y. Han, Z. Wang, X. Wu, Y. Pan, Y. Sun, *ACS Cent. Sci.* **2019**, *5*, 1991.
- [79] L. Li, P. Wang, Q. Shao, X. Huang, *Chem. Soc. Rev.* **2020**, *49*, 3072.
- [80] X. F. Lu, L. Yu, X. W. D. Lou, *Sci. Adv.* **2019**, *5*, eaav6009.
- [81] J. Cai, Y. Song, Y. Zang, S. Niu, Y. Wu, Y. Xie, X. Zheng, Y. Liu, Y. Lin, X. Liu, *Sci. Adv.* **2020**, *6*, eaaw8113.
- [82] H. Zhang, Z. Ma, G. Liu, L. Shi, J. Tang, H. Pang, K. Wu, T. Takei, J. Zhang, Y. Yamauchi, *NPG Asia Mater.* **2016**, *8*, e293.
- [83] M. D. Hossain, Z. Liu, M. Zhuang, X. Yan, G. L. Xu, C. A. Gadre, A. Tyagi, I. H. Abidi, C. J. Sun, H. Wong, *Adv. Energy Mater.* **2019**, *9*, 1803689.
- [84] W. Chen, J. Pei, C. T. He, J. Wan, H. Ren, Y. Wang, J. Dong, K. Wu, W. C. Cheong, J. Mao, *Adv. Mater.* **2018**, *30*, 1800396.
- [85] L. Zhang, Y. Jia, G. Gao, X. Yan, N. Chen, J. Chen, M. T. Soo, B. Wood, D. Yang, A. Du, *Chem* **2018**, *4*, 285.
- [86] H. Zhang, L. Yu, T. Chen, W. Zhou, X. W. Lou, *Adv. Funct. Mater.* **2018**, *28*, 1807086.
- [87] J. Liu, D. Zhu, C. Guo, A. Vasileff, S. Z. Qiao, *Adv. Energy Mater.* **2017**, *7*, 1700518.
- [88] J. Wu, Z. Zhuo, X. Rong, K. Dai, Z. Lebens-Higgins, S. Sallis, F. Pan, L. F. J. Piper, G. Liu, Y. Chuang, Z. Hussain, Q. Li, R. Zeng, Z. Shen, W. Yang, *Sci. Adv.* **2020**, *6*, eaaw3871.
- [89] F. Song, M. M. Busch, B. Lassalle-Kaiser, C.-S. Hsu, E. Petkucheva, M. Bensimon, H. M. Chen, C. Corminboeuf, X. Hu, *ACS Cent. Sci.* **2019**, *5*, 558.
- [90] L. Cao, Q. Luo, J. Chen, L. Wang, Y. Lin, H. Wang, X. Liu, X. Shen, W. Zhang, W. Liu, *Nat. Commun.* **2019**, *10*, 4849.
- [91] X. Su, X.-F. Yang, Y. Huang, B. Liu, T. Zhang, *Acc. Chem. Res.* **2019**, *52*, 656.
- [92] M. Li, H. Wang, W. Luo, P. C. Sherrell, J. Chen, J. Yang, *Adv. Mater.* **2020**, *32*, 2001848.
- [93] S. Lamaison, D. Wakerley, J. Blanchard, D. Montero, G. Rousse, D. Mercier, P. Marcus, D. Taverna, D. Giaume, V. Mougel, *Joule* **2020**, *4*, 395.
- [94] Y. Guo, W. Shi, H. Yang, Q. He, Z. Zeng, J.-Y. Ye, X. He, R. Huang, C. Wang, W. Lin, *J. Am. Chem. Soc.* **2019**, *141*, 17875.
- [95] C. Long, X. Li, J. Guo, Y. Shi, S. Liu, Z. Tang, *Small Methods* **2019**, *3*, 1800369.
- [96] C. Zhao, Y. Wang, Z. Li, W. Chen, Q. Xu, D. He, D. Xi, Q. Zhang, T. Yuan, Y. Qu, *Joule* **2019**, *3*, 584.
- [97] E. Zhang, T. Wang, K. Yu, J. Liu, W. Chen, A. Li, H. Rong, R. Lin, S. Ji, X. Zheng, *J. Am. Chem. Soc.* **2019**, *141*, 16569.
- [98] X. Li, W. Bi, M. Chen, Y. Sun, H. Ju, W. Yan, J. Zhu, X. Wu, W. Chu, C. Wu, Y. Xie, *J. Am. Chem. Soc.* **2017**, *139*, 14889.
- [99] X. Zu, X. Li, W. Liu, Y. Sun, J. Xu, T. Yao, W. Yan, S. Gao, C. Wang, S. Wei, *Adv. Mater.* **2019**, *31*, 1808135.
- [100] Y. Wang, Z. Chen, P. Han, Y. Du, Z. Gu, X. Xu, G. Zheng, *ACS Catal.* **2018**, *8*, 7113.
- [101] L. Han, S. Song, M. Liu, S. Yao, Z. Liang, H. Cheng, Z. Ren, W. Liu, R. Lin, G. Qi, X. Liu, Q. Wu, J. Luo, H. L. Xin, *J. Am. Chem. Soc.* **2020**, *142*, 12563.
- [102] H. Yang, Y. Wu, G. Li, Q. Lin, Q. Hu, Q. Zhang, J. Liu, C. He, *J. Am. Chem. Soc.* **2019**, *141*, 12717.
- [103] M. A. Bañares, *Adv. Mater.* **2011**, *23*, 5293.
- [104] X. Li, H. Y. Wang, H. Yang, W. Cai, S. Liu, B. Liu, *Small Methods* **2018**, *2*, 1700395.
- [105] A. D. Handoko, F. Wei, B. S. Yeo, Z. W. Seh, *Nat. Catal.* **2018**, *1*, 922.
- [106] X. K. Wan, H. B. Wu, B. Y. Guan, D. Luan, X. W. Lou, *Adv. Mater.* **2019**, *31*, 1901349.
- [107] Y. Zhu, J. Wang, H. Chu, Y.-C. Chu, H. M. Chen, *ACS Energy Lett.* **2020**, *5*, 1281.
- [108] S. J. Tinnemans, J. G. Mesu, K. Kervinen, T. Visser, T. A. Nijhuis, A. M. Beale, D. E. Keller, A. M. van der Eerden, B. M. Weckhuysen, *Catal. Today* **2006**, *113*, 3.
- [109] J. Dou, Z. Sun, A. A. Opalade, N. Wang, W. Fu, F. F. Tao, *Chem. Soc. Rev.* **2017**, *46*, 2001.
- [110] B. M. Weckhuysen, *Chem. Soc. Rev.* **2010**, *39*, 4557.

- [111] B. M. Weckhuysen, *Phys. Chem. Chem. Phys.* **2003**, *5*, 4351.
- [112] L. Zhang, Y. Ren, W. Liu, A. Wang, T. Zhang, *Natl. Sci. Rev.* **2018**, *5*, 653.
- [113] M. Askerka, G. W. Brudvig, V. S. Batista, *Acc. Chem. Res.* **2017**, *50*, 41.
- [114] H. Fei, J. Dong, D. Chen, T. Hu, X. Duan, I. Shakir, Y. Huang, X. Duan, *Chem. Soc. Rev.* **2019**, *48*, 5207.
- [115] J. Mao, C.-T. He, J. Pei, W. Chen, D. He, Y. He, Z. Zhuang, C. Chen, Q. Peng, D. Wang, *Nat. Commun.* **2018**, *9*, 4958.
- [116] K. Jiang, M. Luo, M. Peng, Y. Yu, Y.-R. Lu, T.-S. Chan, P. Liu, F. M. F. de Groot, Y. Tan, *Nat. Commun.* **2020**, *11*, 2701.
- [117] H. B. Yang, S.-F. Hung, S. Liu, K. Yuan, S. Miao, L. Zhang, X. Huang, H.-Y. Wang, W. Cai, R. Chen, *Nat. Energy* **2018**, *3*, 140.
- [118] Y. Li, W. Cheng, H. Su, X. Zhao, J. He, Q. Liu, *Nano Energy* **2020**, *77*, 105121.
- [119] A. Westermann, B. Azambre, M. Bacariza, I. Graça, M. Ribeiro, J. Lopes, C. Henriques, *Appl. Catal. B* **2015**, *174*, 120.
- [120] O. Zandi, T. W. Hamann, *Nat. Chem.* **2016**, *8*, 778.
- [121] H. Su, X. Zhao, W. Cheng, H. Zhang, Y. Li, W. Zhou, M. Liu, Q. Liu, *ACS Energy Lett.* **2019**, *4*, 1816.
- [122] W. Z. Su, H. Zhang, W. Zhou, X. Zhao, Y. Li, M. Liu, W. Cheng, Q. Liu, *J. Am. Chem. Soc.* **2020**, *142*, 12306.
- [123] M. Zhong, K. Tran, Y. Min, C. Wang, Z. Wang, C.-T. Dinh, P. De Luna, Z. Yu, A. S. Rasouli, P. Brodersen, *Nature* **2020**, *581*, 178.
- [124] T. Zheng, K. Jiang, N. Ta, Y. Hu, J. Zeng, J. Liu, H. Wang, *Joule* **2019**, *3*, 265.

Manuscript received: October 21, 2020

Accepted manuscript online: December 14, 2020

Version of record online: February 24, 2021